IJMMM International Journal of Minerals, Metallurgy and Materials 矿物冶金与材料学报（英文版）

Comparative review of corrosion-resistant coatings on metal bipolar plates of proton exchange membrane fuel cells

Jiaming Liu, Qian Hu, Sandrick Sabola, Yue Zhang, Biao Du, and Xianzong Wang

Cite this article as:
Jiaming Liu, Qian Hu, Sandrick Sabola, Yue Zhang, Biao Du, and Xianzong Wang, Comparative review of corrosion-resistant coatings on metal bipolar plates of proton exchange membrane fuel cells, *Int. J. Miner. Metall. Mater.*, 31(2024), No. 12, pp. 2627-2644. https://doi.org/10.1007/s12613-024-2946-0

View the article online at SpringerLink or IJMMM Webpage.

Articles you may be interested in

Bao Liu, Shuo Wang, Cheng-yan Wang, Bao-zhong Ma, and Yong-qiang Chen, Electrochemical behavior and corrosion resistance of IrO_2–ZrO_2 binary oxide coatings for promoting oxygen evolution in sulfuric acid solution, *Int. J. Miner. Metall. Mater.*, 27(2020), No. 2, pp. 264-273. https://doi.org/10.1007/s12613-019-1847-0

Wen-rui Wang, Wu Qi, Xiao-li Zhang, Xiao Yang, Lu Xie, Dong-yue Li, and Yong-hua Xiang, Superior corrosion resistance-dependent laser energy density in $(CoCrFeNi)_{95}Nb_5$ high entropy alloy coating fabricated by laser cladding, *Int. J. Miner. Metall. Mater.*, 28(2021), No. 5, pp. 888-897. https://doi.org/10.1007/s12613-020-2238-2

Min Zhu, Qiang Zhang, Yong-feng Yuan, and Shao-yi Guo, Effect of microstructure and passive film on corrosion resistance of 2507 super duplex stainless steel prepared by different cooling methods in simulated marine environment, *Int. J. Miner. Metall. Mater.*, 27(2020), No. 8, pp. 1100-1114. https://doi.org/10.1007/s12613-020-2094-0

Pan-jun Wang, Ling-wei Ma, Xue-qun Cheng, and Xiao-gang Li, Influence of grain refinement on the corrosion behavior of metallic materials: A review, *Int. J. Miner. Metall. Mater.*, 28(2021), No. 7, pp. 1112-1126. https://doi.org/10.1007/s12613-021-2308-0

Navid Mehdipour, Milad Rezaei, and Zeynab Mahidashti, Influence of glycine additive on corrosion and wear performance of electroplated trivalent chromium coating, *Int. J. Miner. Metall. Mater.*, 27(2020), No. 4, pp. 544-554. https://doi.org/10.1007/s12613-020-1975-6

Kuzhipadath Jithesh and Moganraj Arivarasu, Comparative studies on the hot corrosion behavior of air plasma spray and high velocity oxygen fuel coated Co-based L605 superalloys in a gas turbine environment, *Int. J. Miner. Metall. Mater.*, 27(2020), No. 5, pp. 649-659. https://doi.org/10.1007/s12613-019-1943-1

IJMMM WeChat

QQ author group

INTERNATIONAL JOURNAL OF
Minerals, Metallurgy and Materials

Volume 31, Number 12, December 2024
Page 2627

Review https://doi.org/10.1007/s12613-024-2946-0

Comparative review of corrosion-resistant coatings on metal bipolar plates of proton exchange membrane fuel cells

Jiaming Liu[1,2], *Qian Hu*[1,2], *Sandrick Sabola*[2], *Yue Zhang*[3], *Biao Du*[3], *and Xianzong Wang*[1,2]✉

1) Research & Development Institute of Northwestern Polytechnical University in Shenzhen, Shenzhen 518057, China
2) State Key Laboratory of Solidification Processing, Northwestern Polytechnical University, Xi'an 710072, China
3) Shaanxi Coal Chemical Industry Technology Research Institute Co., Ltd., Xi'an 710065, China
(Received: 25 January 2024; revised: 16 May 2024; accepted: 29 May 2024)

Abstract: In the realm of proton exchange membrane fuel cells (PEMFCs), the bipolar plates (BPs) are indispensable and serve pivotal roles in distributing reactant gases, collecting current, facilitating product water removal, and cooling the stack. Metal BPs, characterized by outstanding manufacturability, cost-effectiveness, higher power density, and mechanical strength, are emerging as viable alternatives to traditional graphite BPs. The foremost challenge for metal BPs lies in enhancing their corrosion resistance and conductivity under acidic conditions, necessitating the application of various coatings on their surfaces to ensure superior performance. This review summarizes and compares recent advancements in the research of eight distinct types of coatings for BPs in PEMFCs, including noble metal, carbide, nitride, and amorphous carbon (a-C)/metal compound composite coatings. The various challenges encountered in the manufacturing and future application of these coatings are also delineated.

Keywords: proton exchange membrane fuel cells; metallic bipolar plate; coatings; corrosion resistance; interfacial contact resistance

1. Introduction

Proton exchange membrane fuel cells (PEMFCs) represent the forefront of innovation in the quest for sustainable energy solutions, gaining increasing attention for their high efficiency and minimal emissions [1–2]. Central to the advancement of PEMFCs technology are bipolar plates (BPs), which constitute about 25%–30% of the total cost and 70% of the weight and volume of PEMFCs [3]. These plates are crucial, not only for structural support but also for current collection, heat management, drainage, isolation, and distribution of reactive gases.

Bipolar plates demand a unique combination of properties: strong mechanical strength, high electrical conductivity, robust chemical stability, and excellent air tightness [4]. The materials currently used for BPs fall into three primary categories: graphite-based [5], composite [6], and metal-based [7]. Graphite-based plates, though excellent in electrical conductivity and corrosion resistance, are limited by their brittleness, cost, and lengthy manufacturing process, posing hurdles to widespread commercialization. Meanwhile, composite carbon-based plates, blending polymer resins with carbon conductive fillers, have shown improvements in strength and manufacturability. Yet, they still face critical challenges in electrical conductivity, mechanical robustness, air tightness, and cost efficiency [8–9].

Metal-based bipolar plates, characterized by high strength, good conductivity, and low air permeability, have been successfully integrated into fuel cell stacks by major automotive companies such as Toyota, Hyundai, and General Motors [3]. Numerous alloys have been explored as potential materials for these plates, including stainless steel (SS) [10–11], titanium [12–13], aluminum [14], and nickel alloy [15]. Stainless steel, in particular, is favored for its cost-effectiveness, strength, and ease of mass production [13]. However, the acidic environment (pH: 3–5) and operational temperatures (60–80°C) of PEMFCs can lead to corrosion of the metal matrix. The operating conditions such as high cathodic transient potential induced by SU/SD (start up/shut down), variable loading conditions caused by high loads, and dynamic cycling conditions, all of which can accelerate substrate corrosion. Not only does the generated passivation film diminish the conductivity of the bipolar plates, but also the corrosion-derived metal ions induce catalyst poisoning, affecting both performance and longevity. Therefore, the development of protective coatings that balance corrosion resistance, electrical efficiency, and cost-effectiveness is crucial for the advancement of metal bipolar plates in PEMFCs [4,16].

Coatings and corresponding fabrication techniques are widely used on metal bipolar plates such as noble metal, conductive polymer, carbide, nitride, oxide, and pure carbon coatings to improve their corrosion resistance and reduce their interfacial contact resistance (ICR) [16–17]. In order to compare the advantages and disadvantages of these coatings,

✉ Corresponding author: Xianzong Wang E-mail: xianzong.wang@nwpu.edu.cn
© University of Science and Technology Beijing 2024

six main performance indexes are compared: corrosion resistance, electrical conductivity, adhesion to substrate, long-term service performance stability, production efficiency, and production cost, as shown in Fig. 1. The results of polarization and conductivity tests for different types of coatings, scoring values, and criteria for quantitative scoring can be found in Tables S1 and S2 (see the Supplementray information). For instance, while noble metal coatings demonstrate superior performance in enhancing the efficacy, their high cost remains a significant barrier to widespread adoption. Oxide coatings have the potential to enhance the chemical stability of the coating, but sacrifice the initial conductivity. In summary, each of the predominant 8 categories of coatings exhibits inherent drawbacks that necessitate refinement. Among these, the amorphous carbon (a-C)/metal compound composite coatings are deemed the most promising category for metallic bipolar plate coatings within the existing technical parameters. Besides, internal radar charts for three typical coatings—nitrides, metal compounds, and a-C/metal compound composite coatings—are attached in their respective sections.

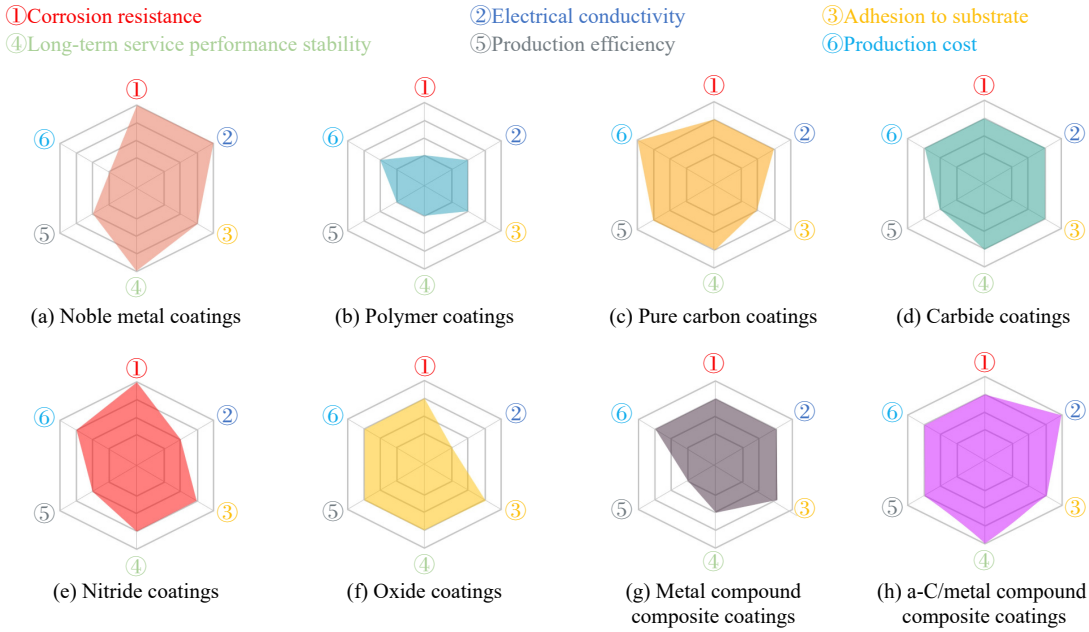

Fig. 1. The performance radar diagrams of different coatings for PEMFCs metal bipolar plates.

In this review, the performance of eight coatings was compared from multiple angles, especially the balance between electrical conductivity and corrosion resistance over long durations. These typical coatings were explored from aspects, such as coating composition, structure, preparation parameters, and performance evaluation methods. The main challenges and development foreground of BPs coatings are also identified, providing reference and guidance for the widespread application of BPs in PEMFCs.

2. Materials and coatings

2.1. Polymer coatings

Conductive polymers, notably polypyrrole (PPY) [18–23], polyaniline (PANI) [22,24–28], along with their derivatives, have gained significant attention in the field of metal bipolar plate coatings due to their excellent chemical and physical stability. Recent years have seen a surge in studies exploring these materials.

A notable study by Akula *et al.* [21] electrosynthesized poly (2-amino-5-mercapto-1,3,4-thiadiazole)/polypyrrole (PAMT/PPY) bilayer polymer composite coating (Fig. 2(a1) and (a2)), showing a dense and compact surface morphology. Potentiodynamic polarization studies indicated that the corrosion current densities (I_{corr}) of PAMT on PPY increased to 25 μA·cm^{-2} (Fig. 2(b)). Fig. 2(c) shows the potentiostatic polarization curves at 0.6 V vs. SCE (Saturated calomel electrode) of PAMT on PPY and PPY on PAMT composite coatings. Although this performance surpasses that of uncoated SS316L, it still falls short of the fundamental requirements for bipolar plate coatings. To further provide corrosion protection of coating through enhanced physical barrier effect and anodic passivation effect, a Nb-doped TiO_2 (Nb–TiO_2) nano-powder modified polyaniline (TNO-PANI) coating was applied on SS316. The tests results showed that the I_{corr} of Nb–TiO_2 nanofiber/PANI composite coating decreased to about 2.75 μA·cm^{-2} in the simulated cathodic environment. However, the current densities at PEMFCs working potential exceeded 1 μA·cm^{-2}, falling short of meeting the DOE (Department of Energy) 2025 technical requirements (Table S3) [24–25].

Liu *et al.* [19] prepared a 6 μm thick polypyrrole (PPY)/graphene (G) composite coating on SS304 surface by cyclic voltammetry to enhance conductivity. The ICR of single PPY and composite PPY/G coatings were 41 mΩ·cm^2 and 19 mΩ·cm^2 at 1.4 MPa pressure, respectively. Despite the decrease in ICR attributed to the outstanding conductivity of graphene and the layered structure of the composite coating,

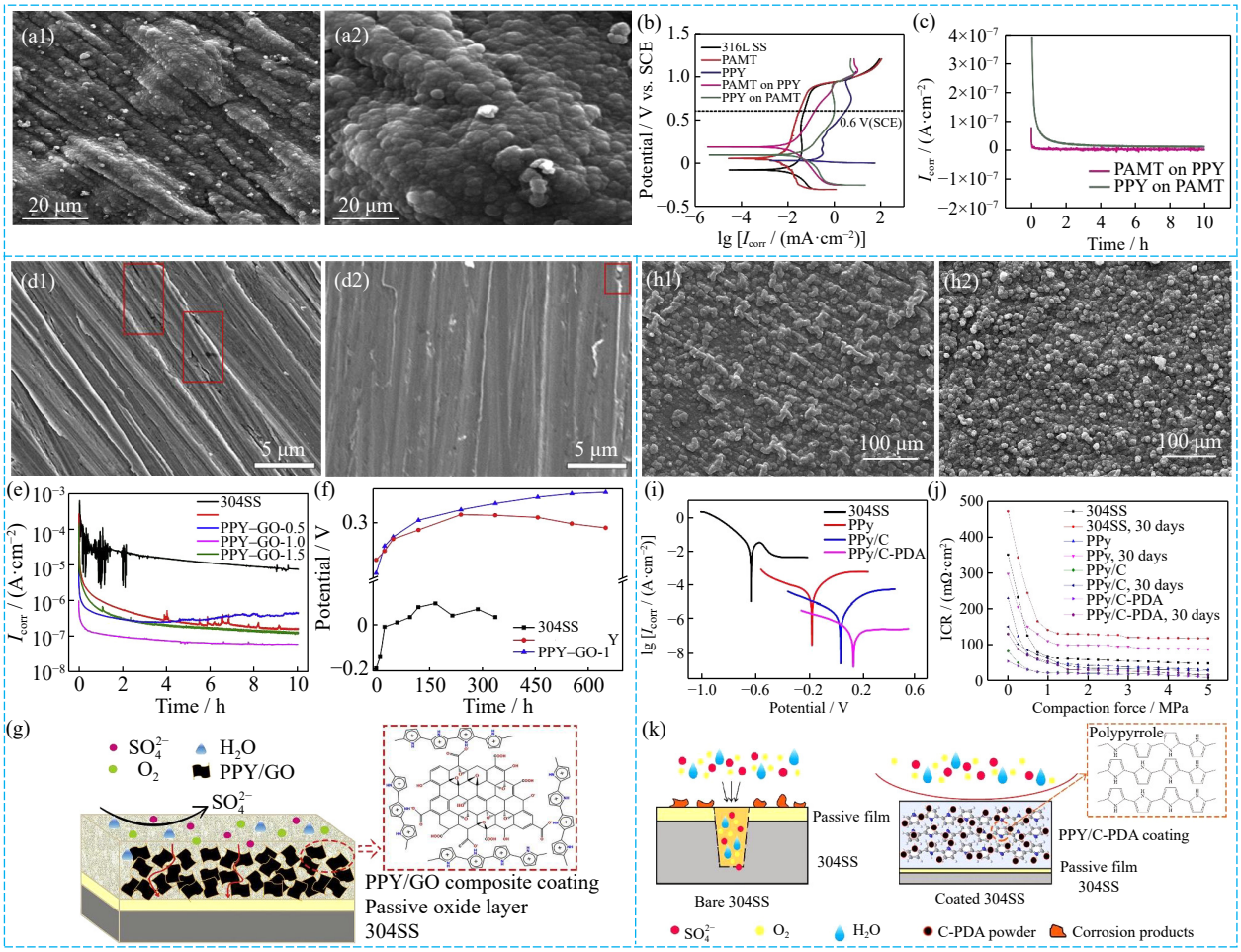

Fig. 2. (a1) and (a2) scanning electron microscope (SEM) images of PAMT on PPY coated SS316L; (b) potentiodynamic polarization curves of PAMT, PPY, PAMT on PPY, and PPY on PAMT composite coatings at cathodic (O_2 purging) environment; (c) potentiostatic polarization curves at 0.6 V vs. SCE of PAMT on PPY and PPY on PAMT composite coatings [21]; (d1) and (d2) respective interfaces beneath PPY and PPY/GO-1 composite coatings after immersion (the boxed area shows the pitting morphologies); (e) potentiostatic tests at 0.6 V vs. SCE; (f) time dependence of opencircuit potential curves; (g) protection mechanism of PPY/GO composite coating [18]; SEM micrographs of (h1) PPY/C and (h2) PPY/C-PDA coated 304 SS after immersion; (i) potentiodynamic polarization results of 304SS, PPY, PPY/C, and PPY/C-PDA; (j) ICR curves of different samples; (k) protection mechanism of PPY/C-PDA composite coating [20]. (a1–c) Reprinted from *Int. J. Hydrogen Energy*, 46, S. Akula, P. Kalaiselvi, A.K. Sahu, and S. Chellammal, Electrodeposition of conductive PAMT/PPY bilayer composite coatings on 316L stainless steel plate for PEMFC application, 17909–17921, Copyright 2021, with permission from Elsevier. (d1–g) Reprinted from *J. Alloys Compd.*, 770, L. Jiang, J.A. Syed, H.B. Lu, and X.K. Meng, *In-situ* electrodeposition of conductive polypyrrole-graphene oxide composite coating for corrosion protection of 304SS bipolar plates, 35–47, Copyright 2019, with permission from Elsevier. (h1–k) Reprinted from *Chem. Eng. J.*, 393, Z.H. Chen, G.H. Zhang, W.Z. Yang, *et al.*, Superior conducting polypyrrole anti-corrosion coating containing functionalized carbon powders for 304 stainless steel bipolar plates in proton exchange membrane fuel cells, 124675, Copyright 2020, with permission from Elsevier.

it still did not meet the DOE's technical benchmarks. Similarly, Jiang *et al.* [18] incorporated graphene oxide (GO) into a polypyrrole (PPY) substrate using *in-situ* electrodeposition on SS304 to prepare PPY/GO composite coatings with different GO content. As depicted in Fig. 2(d1) and (d2), the interface of the PPY/GO-1 composite coating exhibited minimal corrosion, suggesting that this coating provided effective protection to the substrate. Furthermore, the polarization current density of 304 SS coated with PPY/GO-1 was the lowest among the samples, suggesting the most effective and consistent corrosion protection for the 304 SS substrate (Fig. 2(e)–(g)). The coatings prepared by functionalizing carbon powder with polydopamine (PDA) were also investigated for their protective effects on the substrate (Fig. 2(h1)–(k)). After 720 h immersion, the PPY/C-PDA coating appeared more intact than PPY/C coating, featuring distinct spherical structural particles on its surface. Notably, as shown in Fig. 2(j), the stable ICR values of PPY/C-PDA-coated 304 SS initially were 10 mΩ·cm² and increased to 17 mΩ·cm² after 30 d of immersion, suggesting strong potential for PEMFCs applications [20].

In summary, while various conductive polymer coatings, including PPY, PANI, and their composites, have shown promise in providing corrosion resistance, challenges remain in achieving the desired electrical conductivity and meeting DOE targets. The preparation of these coatings often necessitates the addition of other materials to create composites, which could lower polymerization efficiency and increase

costs. Continued innovation and research are essential to develop more efficient and cost-effective polymer coatings for PEMFCs applications.

2.2. Noble metal coatings

Noble metals, notably Ag, Au, and Pt, have been a focal point of research for augmenting the performance of bipolar plates through coating applications [10,29–33]. These metals exhibit remarkable electrical conductivity and corrosion resistance.

Yan *et al*. [30] applied a 0.28 μm Au coating on SS304L, initially treated with Ni for improved Au adhesion. Despite the Au coating's efficacy in preventing SS304 bipolar plate attenuation at 160°C over 432 h, issues such as coating delamination and the prohibitive cost of gold pose practical challenges. To mitigate the high costs associated with noble metals, various studies have explored methods to reduce their usage. These include co-alloying treatments of substrates and doping noble metals into other coatings. Lin *et al*. [29] employed active screen plasma nitrogen–platinum co-alloying (ASPA) on SS316 surfaces with different applied bias, forming dense, columnar single-phase Pt_3Fe layers (Fig. 3(a1)–(a3)). After a 4 h potentiostatic test at 0.6 V vs. SCE, the surface of the 15% Bs (15% applied bias of 15 kVA) sample exhibited no evidence of corrosion compared to the as-treated sample (Fig. 3(b1)–(c)). Moreover, the low I_{corr} and the stable ICR values reflected the great corrosion resistance and chemical stability of Pt_3Fe (Fig. 3(c) and (d)). Unfortunately, the small amount of iron nitride formed during alloying treatment led to the higher passive current density over 10 $\mu A \cdot cm^{-2}$.

Doping noble metals into TiN and a-C coatings has been also studied extensively to alleviate non-negligible degradation caused by corrosion and subsequently increased ICR. For instance, TiN coatings doped with silver nanoparticles were prepared by employing direct current (DC) magnetron sputtering at different temperatures. At 350°C, the coating reached a thickness of 1.198 μm and achieved a prominent ICR of 4.18 $m\Omega \cdot cm^2$, confirming the role of Ag in improving conductivity of TiN coating [31]. Micron spot corrosion Au was also integrated into TiN coatings, which exhibited low corrosion current density of 0.2 $\mu A \cdot cm^{-2}$ at 0.67 V vs. Ag/AgCl for 96 h, and thus presented a stable ICR of 5.8 $m\Omega \cdot cm^2$ after potentiostatic test. Investigation into the dependence of ICRs on Au suggested that 4%–6% surface coverage of Au dots was the critical threshold to meet the target ICR value of 10 $m\Omega \cdot cm^2$. However, subjected to combined cyclic potentiostatic and potentiodynamic polarization, the samples exhibited galvanic corrosion between Au and TiN, subsequently significant delamination of Au dots (Fig. 3(e1)–(f)) [10]. Following this, Zhang *et al*. [32] furthered this approach by doping a-C coating with Ag and Cr using closed field unbalanced magnetron sputter ion plating (CFUBMSIP) (Fig. 3(g)). Similarly, galvanic corrosion between Ag and a-C also occurred in the coatings with higher Ag and Cr concentrations, resulting in deteriorated corrosion resistance after durability corrosion tests. The potentiostatic curves and ICR data corroborate the improved durability and reduced ICR with moderate Ag and Cr content (Fig. 3(h)–(j)).

In summary, while noble metal coatings demonstrate superior performance in enhancing the efficacy of bipolar plates in PEMFCs, their high cost remains a significant barrier to widespread adoption. Doping noble metals into corrosion-resistance coatings has been confirmed to effectively alleviate the rapid degradation of conductivity during the corrosion process, but galvanic corrosion might induce the noble metal ion release, especially under combined potential polarization. This underscores the need for cost-effective yet high-performing alternatives in bipolar plate technology.

2.3. Pure carbon coatings

Pure carbon coatings, recognized for their exceptional electrical conductivity, corrosion resistance, chemical inertness, and mechanical hardness have garnered significant interest for enhancing the performance of metal BPs [34–41]. Numerous researchers have explored the application of these coatings to assess the enhancement in the performance of metal BPs.

For instance, Fukutsuka *et al*. [34] fabricated a carbon coating on SUS304 surface through plasma-assisted chemical vapor deposition. The resulting ICR of the carbon coating measured approximately 8.9 $m\Omega \cdot cm^2$ at 1 MPa, highlighting its potential in reducing ICR. Exploring the influence of substrate variations, Li *et al*. [41] developed a-C coatings on SS316L and TA2 by DC balanced magnetron sputtering. X-ray photoelectron spectroscopy (XPS) spectra analysis revealed sp2 bonding proportions of 56.06% and 57.75% for the a-C films on TA2 and SS316L substrates, respectively (Fig. 4(a1) and (a2)). This elevated sp2 content correlated with a reduced ICR, which dropped to 5.64 and 6.52 $m\Omega \cdot cm^2$ at 1.5 MPa for the respective substrates (Fig. 4(b)). Potentiostatic polarization tests demonstrated a substantial reduction in current density for the a-C-coated SS316L and TA2 samples, meeting the DOE target at 0.6 V vs. SCE (Fig. 4(c)–(d2)).

The impact of the preparation temperature on the protective effect on the substrate has also been noted. Afshar *et al*. [35] investigated the effects of varying substrate temperatures (100–500°C) on the structural, chemical, and electrical properties of carbon coatings on SS316L. Their findings revealed that the corrosion resistance decreased at elevated temperatures due to the emergence of cracks and pores, with optimal resistance observed at temperatures below 400°C. The most effective performance was achieved at a substrate temperature of 300°C, where the carbon coating exhibited superb corrosion resistance. Building on this, Li *et al*. [38] further demonstrated that the microstructure of a-C nano-coatings could be altered by varying the deposition temperature during magnetron sputtering. They observed a transition from a columnar to a dense microcrystalline structure in the a-C nano-coating when the deposition temperature exceeded 300°C (Fig. 4(e1) and (e2)). This change also led to an in-

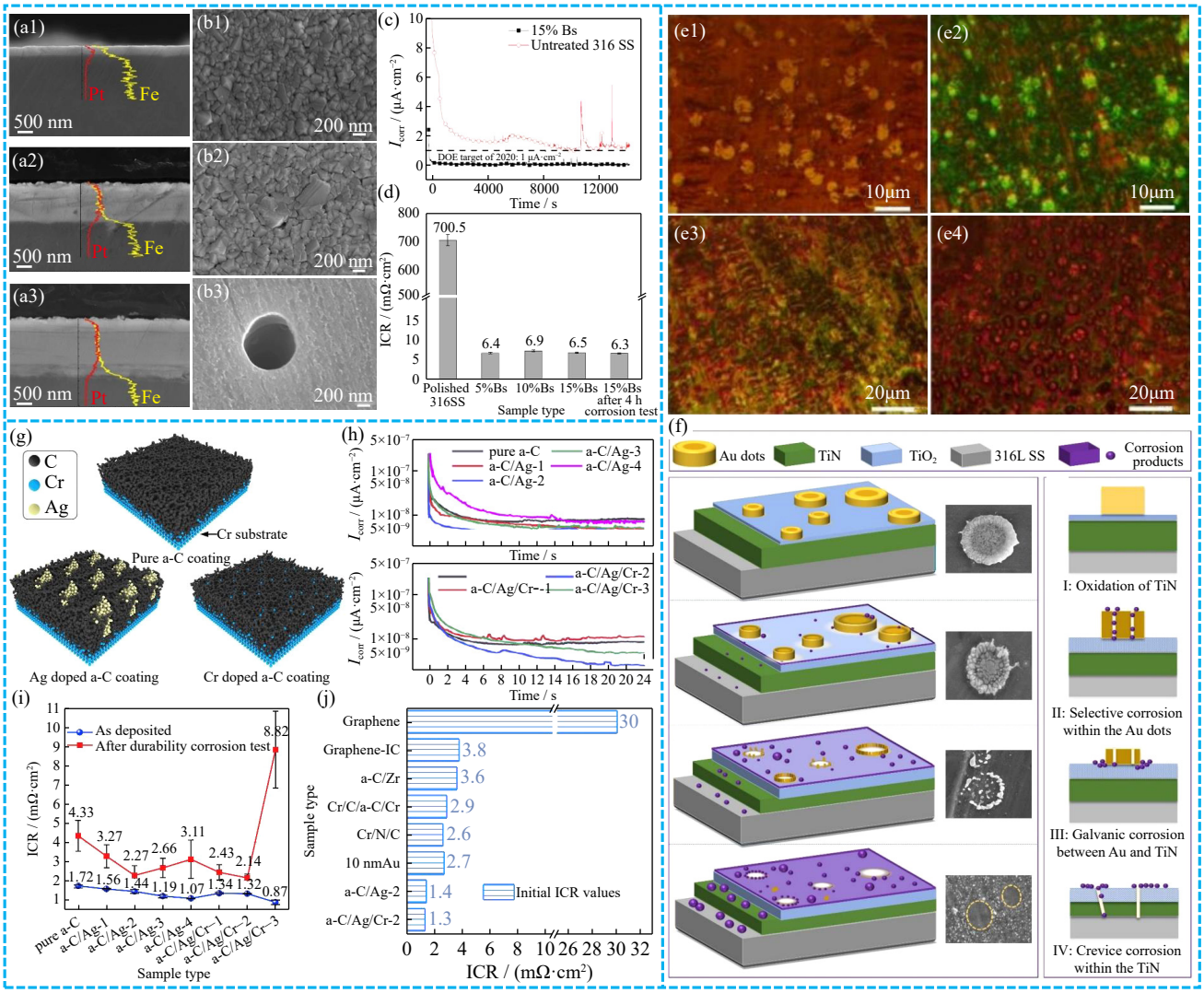

Fig. 3. Cross-sectional SEM images of ASPA(N+Pt) treated samples: (a1) 5%Bs; (a2) 10%Bs; (a3) 15%Bs; Surface morphology of (b1) 15%Bs before polarization, (b2) 15%Bs, and (b3) untreated 316 SS after potentiostatic test at 0.6 V vs. SCE; (c) Potentiostatic polarization curves of 15%Bs and untreated 316SS; (d) ICR data [29]; Optical microscopy images of Au/TiN/SS after (e1) 24, (e2) 36, (e3) 48, and (e4) 60 h tests; (f) Schematic diagram of the cyclic combined potential induced dissolution of Au/TiN/SS [10]; (g) Simulated structure of typical doped a-C coatings; (h) Potentiostatic tests at 0.6 V vs. Ag/AgCl; (i) ICR curves; (j) Several typical as-deposited ICR [32]. (a1–d) Reprinted from *Int. J. Hydrogen Energy*, 42, K.J. Lin, X.Y. Li, H.S. Dong, *et al.*, Surface modification of 316 stainless steel with platinum for the application of bipolar plates in high performance proton exchange membrane fuel cells, 2338–2348, Copyright 2017, with permission from Elsevier. (e1–f) Reprinted from *Corros. Sci.*, 189, X.Z. Wang, C.P. Ye, D.D. Shi, H.Q. Fan, and Q. Li, Potential polarization accelerated degradation of interfacial electrical conductivity for Au/TiN coated 316L SS bipolar plates used in polymer electrolyte membrane fuel cells, 109624, Copyright 2021, with permission from Elsevier. (g–j) Reprinted from *Carbon*, 145, D. Zhang, P.Y. Yi, L.F. Peng, X.M. Lai, and J.B. Pu, Amorphous carbon films doped with silver and chromium to achieve ultra-low interfacial electrical resistance and long-term durability in the application of proton exchange membrane fuel cells, 333–344, Copyright 2019, with permission from Elsevier.

creased content of sp2 carbon in the coating, significantly enhancing its corrosion resistance, interface conductivity, and hydrophobicity.

Li *et al.* [36] extended this research by depositing a series of a-C coatings on SS316L samples using magnetron sputtering technology at different power levels. The sample prepared at 0.9 kW exhibited the best corrosion resistance, as evidenced by the stable current density gradually increasing from 3.99×10^{-3} μA·cm^{-2} at 0.9 kW to 2.948×10^{-2} μA·cm^{-2} at 2.1 kW (Fig. 4(f) and (g)). Post long-term potentiostatic testing, the morphology and element distribution of the a-C film remained stable (Fig. 4(h)). However, the presence of spherical defects enriched in Cr and O elements at the interface suggested a potential alternative corrosion mechanism within the a-C coating, potentially leading to the formation of Cr_2O_3 spherical defects (Fig. 4(i)). Furthermore, a novel approach involved preparing a graphite sheet on the SS316L substrate, transforming it into continuous graphite through rapid heating between 800 and 900°C. The resulting graphite displayed a loosely porous structure and was used to create a pure graphite coating atop a binder layer, forming a pinhole-free protective film with superior electrical conductivity

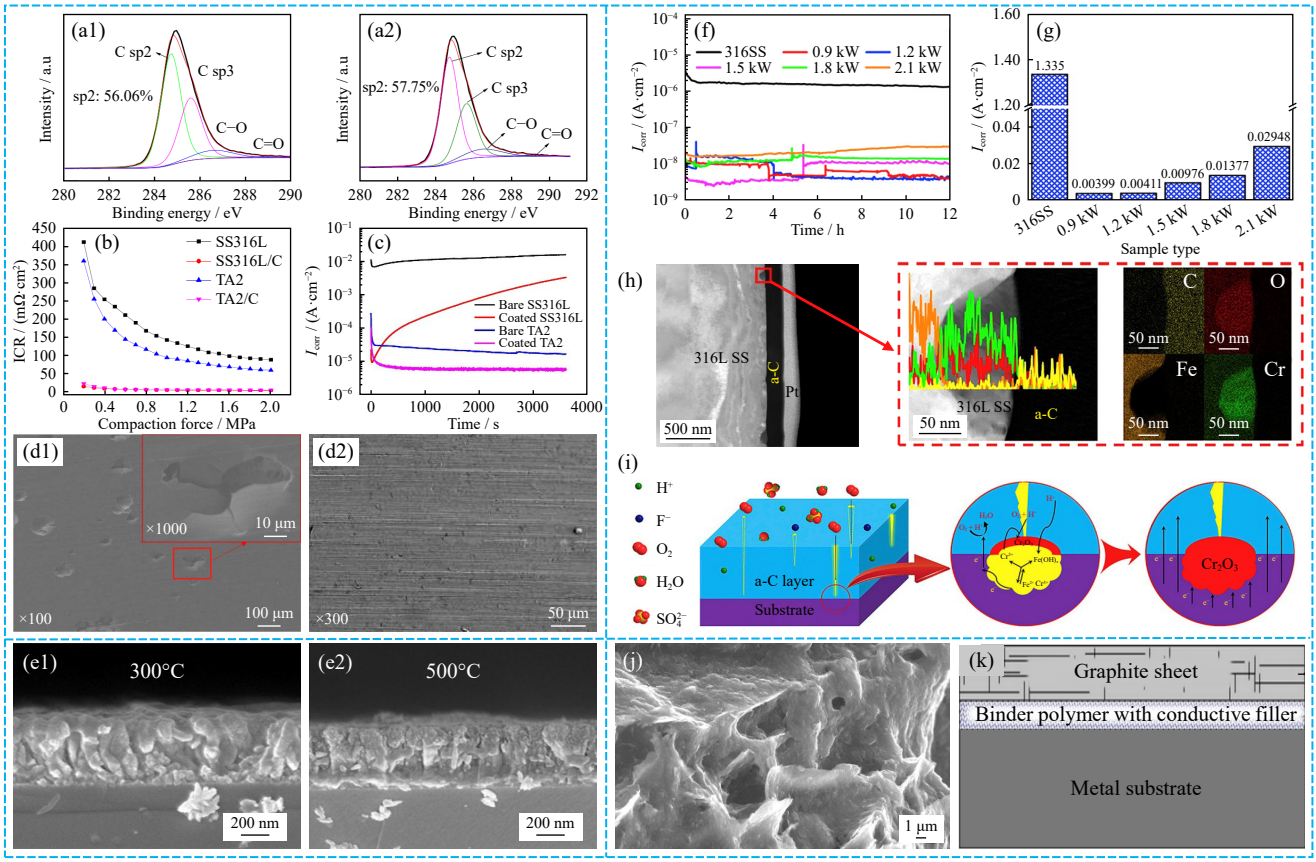

Fig. 4. XPS spectra of the a-C films on (a1) TA2 and (a2) SS316L; (b) ICR values of SS316L, SS316L/C, TA2, and TA2/C; (c) potentiostatic tests of bare SS316L, coated SS316L, bare TA2, and coated TA2 at 1.4 V vs. SCE; SEM images after potentiostatic tests at 1.4 V vs. SCE: (d1) coated SS316L and (d2) coated TA2 [41]; SEM images of a-C nano-coatings: (e1) 300°C, (e2) 500°C [38]; (f) potentiostatic tests of 316SS and 0.9–2.1 kW deposited samples at 0.6 V vs. Ag/AgCl, and (g) corresponding stable current densities; (h) high angle annular dark field (HAADF) images of the 0.9 kW-deposited a-C films, and the energy-dispersive spectroscopy (EDS) line-scanning map after the potentiostatic tests; (i) schematic of possible interface-induced degradation mechanism of the a-C films [36]; (j) SEM micrographs of the graphite flake; (k) schematic illustration of the graphite-coated plates [37]. (a1–d2) Reprinted from *Diamond Relat. Mater.*, 118, W. Li, L.T. Liu, Z.X. Li, Y.F. Wang, H.Z. Li, and J.J. Lei, Corrosion resistance and conductivity of amorphous carbon coated SS316L and TA2 bipolar plates in proton-exchange membrane fuel cells, 108503, Copyright 2021, with permission from Elsevier. (e1) and (e2) Reprinted from *Int. J. Electrochem. Sci.*, 18, L.X. Li, D.H. Ye, Y. Xiang, and W. Guo, Effect of deposition temperature on columnar structure of α-C nano-coatings of PEMFC metal bipolar plates, 100188, Copyright 2023, with permission from Elsevier. (f–i) Reprinted from *J. Power Sources*, 469, H. Li, P. Guo, D. Zhang, *et al.*, Interface-induced degradation of amorphous carbon films/stainless steel bipolar plates in proton exchange membrane fuel cells, 228269, Copyright 2020, with permission from Elsevier. (j) and (k) Reprinted from *Electrochim. Acta*, 62, W.L. Wang, S.M. He, and C.H. Lan, Protective graphite coating on metallic bipolar plates for PEMFC applications, 30–35, Copyright 2012, with permission from Elsevier.

(Fig. 4(j) and (k)). The potentiodynamic polarization results, even after prolonged immersion tests, maintained a remarkably low corrosion current density, adhering to the DOE target [37].

In summary, pure carbon coatings demonstrate considerable potential in enhancing the performance of metal BPs, particularly due to their superior electrical conductivity and corrosion resistance. However, challenges remain, notably the adhesion issues between carbon layers and metal substrates, which can lead to delamination over extended service periods. Moreover, the high production costs of materials like amorphous carbon and graphene present barriers to large-scale manufacturing. Ongoing research is essential to overcome these challenges, focusing on improving adhesion properties and reducing production costs, thereby making pure carbon coatings a more feasible and economical option for industrial applications.

2.4. Carbide coatings

Carbide coatings [42–49] are renowned for their superior corrosion resistance and electrical conductivity. They are increasingly being favored as the primary option for metal bipolar plate coatings in both academic and industrial spheres, owing to their superior performance and cost-effectiveness. Presently, carbide coatings stand as one of the most extensively researched and widely used metal bipolar plate coatings.

Jin *et al.* [42] prepared CrAlCN coatings with different carbon contents on the SS316L substrate by using closed field unbalanced magnetron sputter ion plating (CFUMSIP). The C-12sccm sample showed the lowest ICR values of 2.94 and 7.42 mΩ·cm^2 before and after corrosion at 1.4 MPa. This

underscores the effectiveness of the CrAlCN coatings in enhancing surface conductivity, which is due to its highest carbide content. Similarly, Mo–C coatings of varying thicknesses were manufactured on SS316L by magnetron sputtering. Their results demonstrated that increasing the coating thickness improved corrosion resistance. A thin transition layer of Cr on SS316L prior to Mo–C deposition further enhanced performance by eliminating micro-defects [43]. Hou *et al*. [45] prepared a series of a-C films (a-C:Cr) with varying Cr content on SS316L, observing an initial decrease and subsequent increase in resistance with higher Cr content, suggesting an optimum Cr concentration for maximizing conductivity. Additionally, multilayer Cr–C coatings were prepared on SS316L using CFUBMSIP (Fig. 5(a)). The $Cr_{0.75}C_5$ coating exhibited an I_{corr} of 1.046 μA · cm^2 at 0.6 V vs. SCE, demonstrating outstanding corrosion resistance, likely due to the higher proportion of C sp2, enhancing the coating's corrosion resistance. Moreover, the potentiostatic experiments at 0.6 V vs. SCE show the stability of the coating film. Notably, the ICR results indicated a significant improvement in electrical conductivity with this coating (Fig. 5(b)–(d)) [44].

The MXene analogous phase (MAX), a novel material distinct from traditional transition metal carbide coatings, offers excellent oxidation resistance and electrical conductivity due to its unique layered structure and bonding characteristics. Lu *et al*. [46] deposited multilayer Ti–Al–C thin films on 304 SS substrates using physical vapor deposition (PVD), subsequently forming a Ti_3AlC_2 phase through annealing

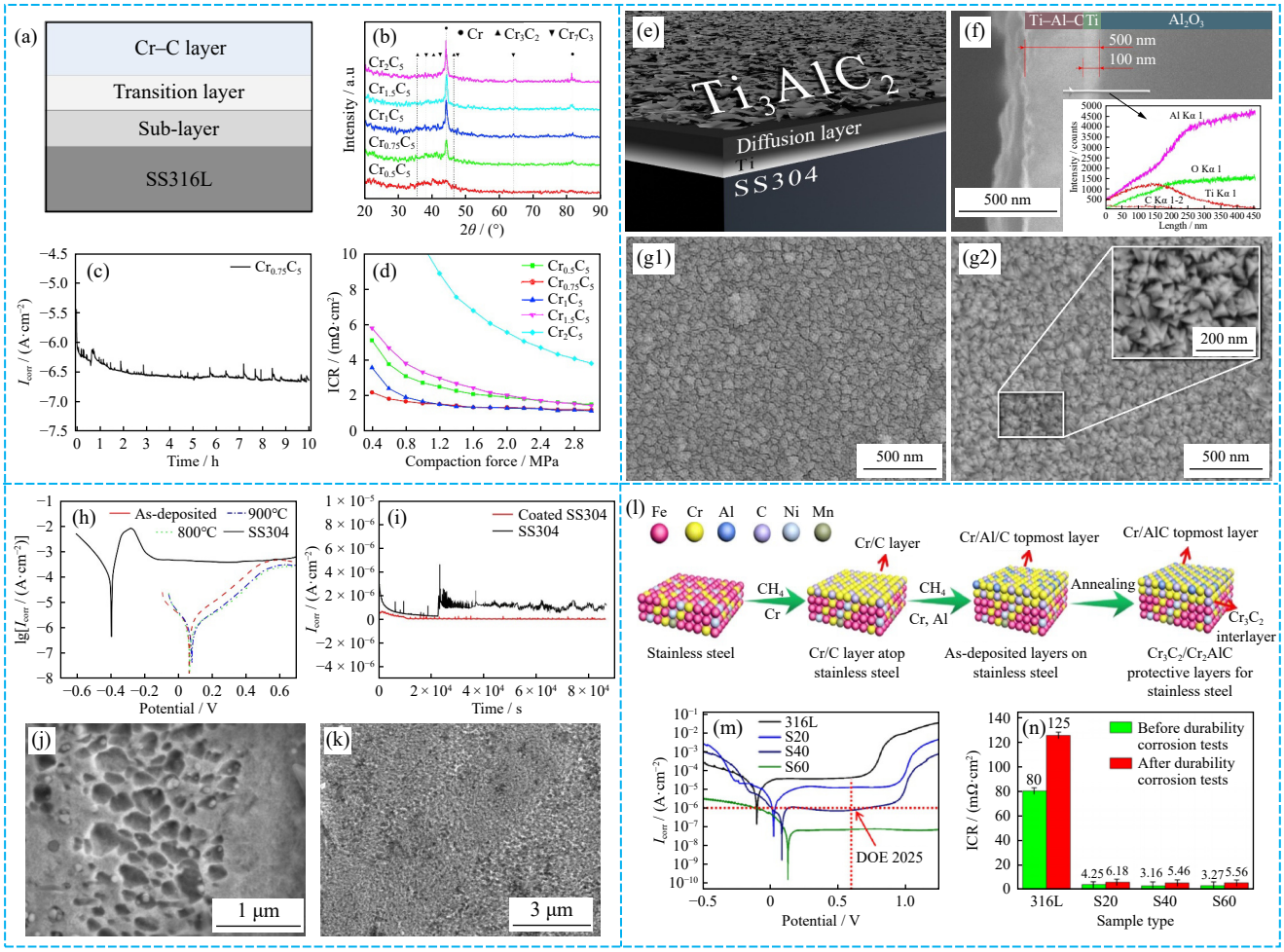

Fig. 5. (a) Schematic diagram of Cr–C film; (b) XRD patterns of the Cr–C multilayer films; (c) potentiostatic tests curves of $Cr_{0.75}C_5$; (d) ICR curves of Cr–C coated SS316L samples [44]; (e) schematic illustration of Ti/–Al–C multilayer film; (f) EDS line analysis of cross-sections of Ti–Al–C films; surface SEM images of heat-treated Ti–Al–C-coated SS304 at (g1) 800 and (g2) 900°C; (h) potentiodynamic polarization curves of bare SS304 and coated SS304 samples; (i) potentiostatic tests of bare SS304 and the Ti_3AlC_2 coated SS304 at 0.6 V vs. SCE for 24 h; (j) SEM images of bare SS304 after potentiostatic tests; (k) SEM images of Ti_3AlC_2-coated SS304 [46]; (l) schematic illustration of Cr_2AlC layer; (m) potentiodynamic curves of 316L, S20, S40, and S60; (n) ICR values of 316L, S20, S40, and S60 before and after the tests [47]. (a–d) Reprinted from *Int. J. Hydrogen Energy*, 41, Y. Zhao, L. Wei, P.Y. Yi, and L.F. Peng, Influence of Cr–C film composition on electrical and corrosion properties of 316L stainless steel as bipolar plates for PEMFCs, 1142–1150, Copyright 2016, with permission from Elsevier. (e–k) Reprinted from *Corros. Sci*., 158, J.L. Lu, N. Abbas, J.N. Tang, J. Tang, and G.M. Zhu, Synthesis and characterization of conductive ceramic MAX-phase coatings for metal bipolar plates in simulated PEMFC environments, 108106, Copyright 2019, with permission from Elsevier. (l–n) Reprinted from *J. Mater. Sci. Technol*., 105, G.S. Ma, D. Zhang, P. Guo, *et al.*, Phase orientation improved the corrosion resistance and conductivity of Cr_2AlC coatings for metal bipolar plates, 36–44, Copyright 2022, with permission from Elsevier.

(Fig. 5(e)). With the rise in heating temperature from 800 to 900°C, there was a corresponding increase in grain size from 10 to 50 nm, indicating that elevated provided greater energy to fostered grain growth (Fig. 5(f)–(g2)). The Ti_3AlC_2-coated sample exhibited outstanding corrosion resistance with an average current density of 0.8 μA·cm^2 in potentiostatic polarization tests at 0.6 V vs. SCE. Furthermore, the exceptionally lower ICR, when compared to other samples, underscores its outstanding conductivity (Fig. 5(h)–(k)). To investigate the impact of phase orientation on the corrosion resistance and conductivity of bipolar plates, the Cr_2AlC coatings with different crystal orientations were prepared by arc/sputtering deposition combined with vacuum annealing (Fig. 5(l)). The S60 sample showed the best corrosion resistance, with the lowest I_{corr} of 0.068 μA·cm^2 (Fig. 5(m)). Density functional calculations suggested that the preferential orientation (103) of the Cr_2AlC layer facilitated the formation of an oxide layer, contributing to its superior corrosion resistance. Additionally, the S60 sample maintained remarkably low ICR before and after potentiostatic polarization (Fig. 5(n)) [47].

In summary, while carbide coatings show immense potential, their long-term electrical conductivity and preparation efficiency warrant further improvement. The stringent conditions required for temperature and carbon sources during the preparation pose significant challenges for large-scale production, highlighting a critical area for future research and development.

2.5. Nitride coatings

Nitride coatings [50–55], such as titanium nitride (TiN), chromium nitride (CrN), and titanium aluminum nitride (TiAlN), have garnered considerable attention in recent years for their robust structural and mechanical properties. These coatings hold particular appeal for deployment in metal bipolar plates across various technological applications, owing to their dense surface structure, exceptional protective qualities, good corrosion resistance, and superior surface conductivity.

In order to explore novel metal compound coatings, the TiN coatings using titanium tetra (dimethylamino) (TDMAT) and titanium tetrachloride ($TiCl_4$) as precursors were prepared by plasma-enhanced atomic layer deposition (PEALD). The TDMAT-TiN coating provided more effective protection for SS316L than $TiCl_4$-TiN, achieved a positive corrosion potential (E_{corr}) of –0.263 V vs. SCE and a low I_{corr} of 0.1 μA·cm^{-2} (Fig. 6(a1)–(b)). The higher I_{corr} of $TiCl_4$-TiN coating was attributed to the presence of Cl and Fe within the bulk films, as indicated by the Auger electron spectroscopy (AES) depth profile and energy-dispersive X-ray spectroscopy (EDX) mapping analysis (Fig. 6(c) and (d)) [54]. Following this research, Jang *et al*. [53] modified the surface of SS316L by depositing 4.5 μm of Ta and 200 and 400 nm of TiN using magnetron sputtering and plasma-enhanced atomic layer deposition, respectively (Fig. 6(e)). As a result, the I_{corr} at 0.6 V vs. SCE was reduced to 1.3, 1.0 μA·cm^{-2} for TaTiN200 and TaTiN400, respectively (Fig. 6(f)). Besides, the ICR values of TaTiN400 sample declined to 7.78 mΩ·cm^2, thus meeting the DOE 2025 targets for ICR (Fig. 6(g)). By disproportionation reaction of Nb(IV) ions in NaCl–KCl–NaF molten salt, Yang *et al*. [11] successfully synthesized a dense nanocrystalline β-Nb_2N coating with thickness of about 600 nm, which was composed of nanocrystalline grains with an average size of ~30 nm (Fig. 6(h)–(j)). Notably, 500 h long-term polarization at 0.23 V vs. MSE (mercurous sulfate electrode) was carried out on the sample (Fig. 6(k)). The current density was quite stable at around 0.15 μA·cm^{-2}. More importantly, the ICR of β-Nb_2N coating after long-term polarization was only 5.2 mΩ·cm^2, reflecting the high chemical stability and robust protection of the β-Nb_2N coating. Mi *et al*. [55] doped CrTiN coatings with different C content on SS316L, wherein a-C and chromium carbide phases appeared as the C target current increased from 0 to 6 A. At 1.1 V vs. SHE (saturation hydrogen electrode) potentiostatic polarization for 2 h, the current density of C-6A sample was stable at a minimum value of 0.609 μA·cm^{-2}. Additionally, the ICR slightly decreased to 7.6 mΩ·cm^2 after polarization, indicating outstanding corrosion resistance and electrical conductivity at high potential.

In conclusion, the overall characteristics of nitride coatings are remarkable (Fig. 7), and the properties of various metallic nitrides have emerged as a pivotal focus in contemporary research endeavors. Nevertheless, thermodynamically, the corrosion dissolution of the nitride compound in an acidic solution and the subsequent oxidation of the coating over prolonged service durations may contribute to the increase of the ICR.

2.6. Oxide coatings

Metal oxides, relatively simple to employ as coatings for bipolar plates (BPs) [56–63] have evolved from early surface treatment technologies that utilized oxide films formed on the metal BPs as protective layers. Profiting from the high transpassivation potential of metal oxides, this coating generally has improved corrosion resistance, while this approach often could not guarantee satisfactory conductivity.

Pillis *et al*. [58] deposited two types of Nb_2O_5 coatings on SS316L by magnetron sputtering for 15 and 30 min, respectively. Peak fitting of Nb 3d spectra indicated two different oxidation states, Nb^{4+} and Nb^{5+}. The corrosion current density and anodic current density of the film for 15 min sample at room temperature were relatively low, which linked to surface enrichment of the less reactive Nb^{5+}. Despite their excellent corrosion resistance, the doped oxide coatings did not achieve optimal conductivity levels. Aiming to enhance both corrosion resistance and conductivity, the multilayer CrO*/Cr coatings were prepared on 304 SS substrate using magnetron sputtering with a remote inductively coupled oxygen plasma (O-ICP) (Fig. 8(a) and (b)) [59]. Compared to the native oxide layer, the CrO*/Cr/SS exhibited a lower stable corrosion current density (<1 μA·cm^{-2}), attributed to the ox-

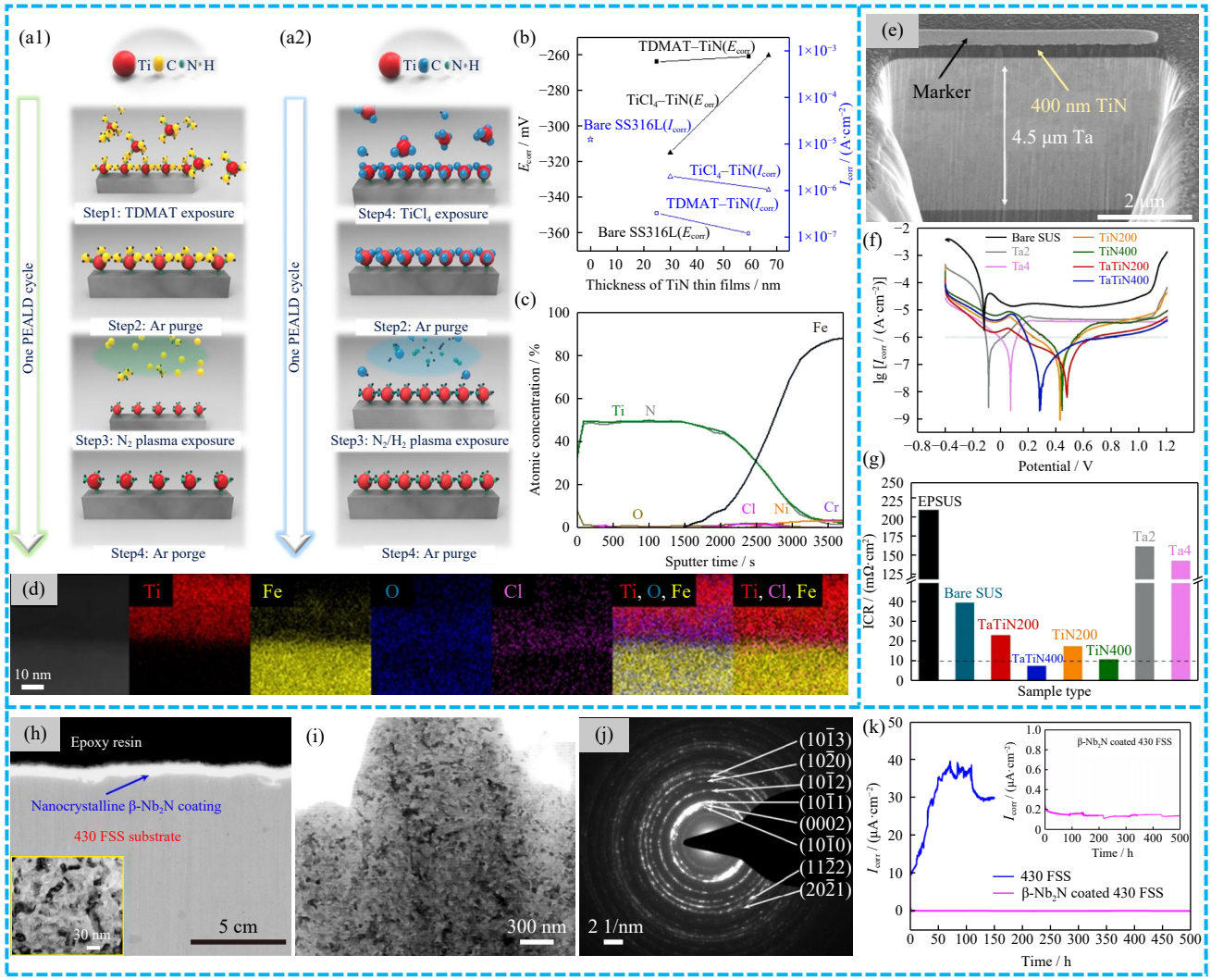

Fig. 6. Schematic of TiN coating prepared by PEALD: (a1) process using the TDMAT precursor and an N_2 plasma, (a2) process using the $TiCl_4$ precursor and an N_2/H_2 plasma; (b) calculated E_{corr} and I_{corr}; (c) AES depth profiles of the $TiCl_4$–TiN thin films deposited with 1050 PEALD cycles; (d) dark-field TEM images with EDX element mapping of $TiCl_4$–TiN deposited using 400 PEALD cycles [54]; (e) SEM images of TaTiN400; (f) potentiodynamic polarization curves of different samples; (g) ICR data of different samples [53]; (h) morphologies of β-Nb_2N coating on 430 ferritic stainless steel (FSS) substrate, the inset shows HRTEM images of the β-Nb_2N coating; (i) TEM image and (j) corresponding selected area electron diffraction (SAED) pattern of β-Nb_2N coating; (k) potentiodynamic tests of uncoated and β-Nb_2N coated 430 FSS [11]. (a1–d) Reprinted from *Appl. Surf. Sci.*, 519, W.J. Lee, E.Y. Yun, H.B.R. Lee, S.W. Hong, and S.H. Kwon, Ultrathin effective TiN protective films prepared by plasma-enhanced atomic layer deposition for high performance metallic bipolar plates of polymer electrolyte membrane fuel cells, 146215, Copyright 2020, with permission from Elsevier. (e–g) Reprinted from *J. Alloys Compd.*, 977, Y. Jang, Y. Kim, W. Jeong, *et al.*, Corrosion behavior of Ta and TiN double-layer-coated SUS316L for PEMFC bipolar plates using plasma-enhanced atomic layer deposition and magnetron sputtering, 173379, Copyright 2024, with permission from Elsevier. (h–k) Reprinted from *Corros. Sci.*, 174, L.X. Yang, R.J. Liu, Y. Wang, H.J. Liu, C.L. Zeng, and C. Fu, Growth of nanocrystalline β-Nb_2N coating on 430 ferritic stainless steel bipolar plates of PEMFCs by disproportionation reaction of Nb(IV) ions in molten salt, 108862, Copyright 2020, with permission from Elsevier.

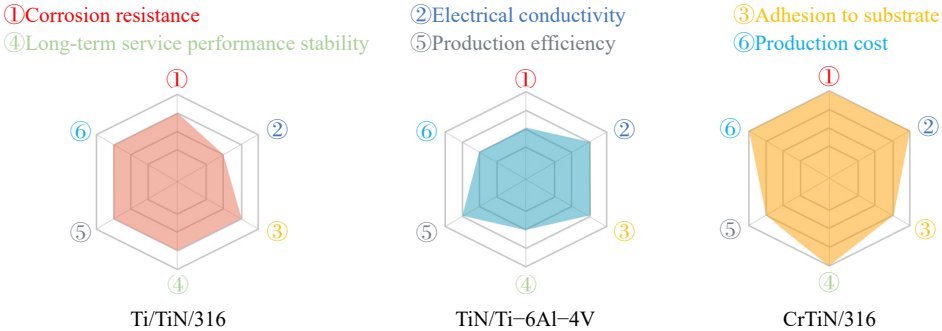

Fig. 7. Performance radar diagrams of three representative nitride coatings.

idation of Cr to its highest valence state in CrO* layer (Fig. 8(c)). While the introduction of oxygen initially reduced conductivity, the CrO*/Cr/SS specimens demonstrated slower conductivity decay during polarization and better conductivity retention post-testing (Fig. 8(d)).

Subsequent studies by Wang *et al*. [61] involved introducing controlled amounts of oxygen into ZrN coatings using plasma-enhanced atomic layer deposition to create Zr_2N_2O conductive coatings (Fig. 8(e1)–(j)). As Fig. 8(i) shows, the ICRs of Zr_2N_2O/SS before and after 42 h intermittently polarization at 0.6 V vs. Ag/AgCl are 6.9 and 12.5 mΩ·cm^2, respectively. Additionally, as Fig. 8(j) shows, the introduction of oxygen increases the oxidation resistance of ZrN, thereby limiting the thickness of the oxide layer and reducing the corrosion products on the surface due to the reduced corrosion current density, so the ICR after long-term test of Zr_2N_2O/SS was much lower than that of ZrN/SS. At a cathodic transient potential as positive as 1.1 V vs. Ag/AgCl, the substrate is effectively protected by the Zr_2N_2O coating [62]. As a result, Zr_2N_2O reduces the anodic dissolution of 304 SS in the transpassive region. These coatings effectively protect the substrate, as evidenced by minimal shallow corrosion pits after long-term polarization (Fig. 8(e1) and (e2)). The Zr_2N_2O coatings, with a wider bandwidth than the passivation film on 304 SS, required a higher anodic polarization potential to "bend" the valence band upwards to reach the E_F and thus enter the transpassive region at a more positive potential than 304 SS. In summary, it was proved that introducing a controlled amount of oxygen could alleviate the oxidation of the coating during polarization, thus inhibit the ICR attenuation rate of the coating (Fig. 8(f) and (g)).

Besides the studies above, the TiNO coatings with varying oxygen contents were fabricated on 316L SS using CFUMSIP [60]. Worth mentioning is that a SU/SD (start up/shut down) cycle test was designed to evaluate the durability of the bipolar plate coatings, involving 6000 cycles of a

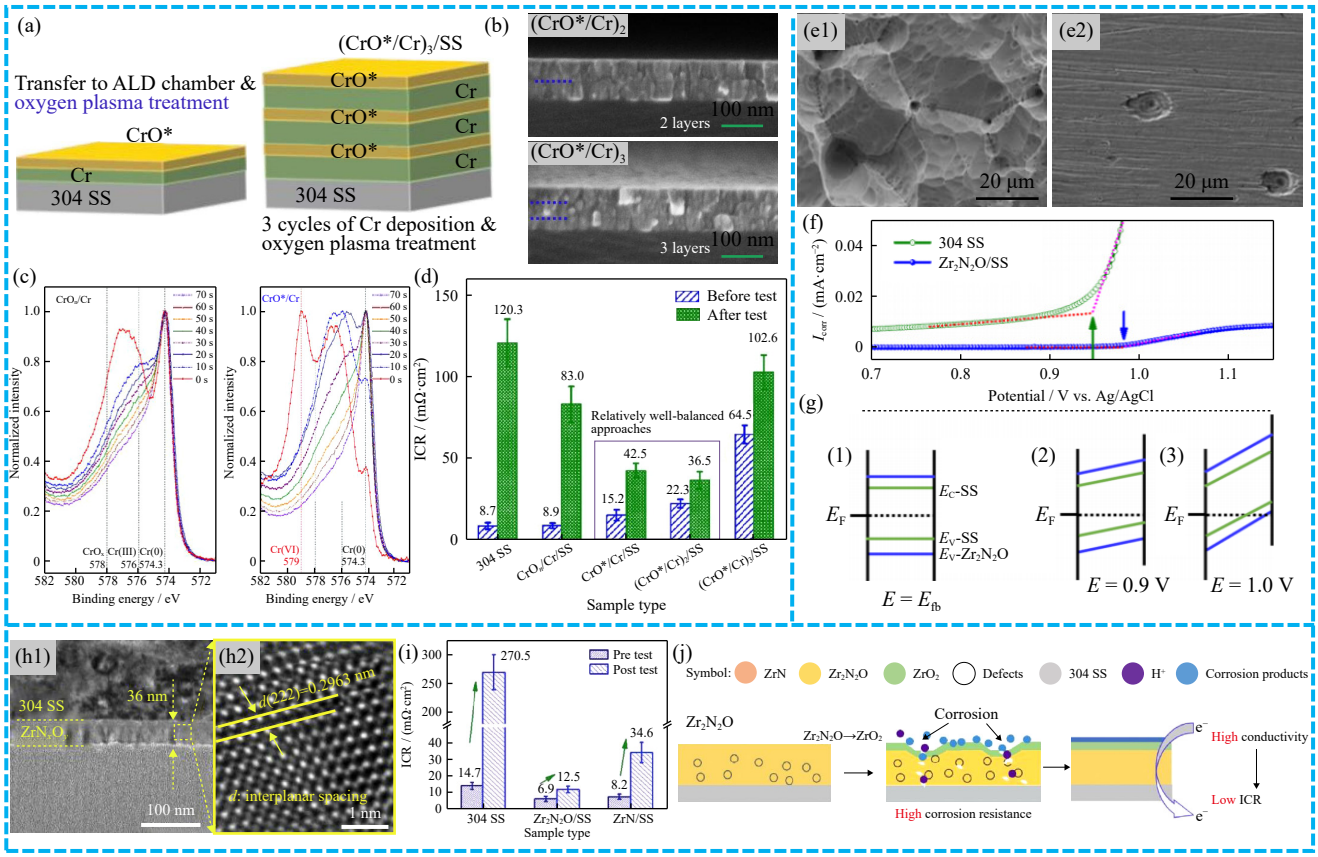

Fig. 8. (a) Schematic diagram of the CrO*/Cr coatings, (b) cross-sectional SEM images of $(CrO*/Cr)_2$ and $(CrO*/Cr)_3$; (c) XPS spectra of Cr 2p of CrO_n/Cr and CrO*/Cr; (d) ICR data [59]; surface morphologies of the 304 SS (e1) and Zr_2N_2O/SS (e2) after long-term test; comparison of the (f) potentiodynamic curves and (g) electron energy level diagrams with the applied potentials of 304 SS and Zr_2N_2O/SS fermi level (E_F), valence band maximum (E_V), conduction band minimum (E_C), flat band potential (E_{fb}), applied potential (E) [62]; (h1) and (h2) cross-sectional FIB-TEM images of the Zr_2N_2O/SS ; (i) ICR results of different samples before and after the tests; (j) electrochemical process of the ZrN and Zr_2N_2O and its effect on the ICR after test [61]. (a–d) Reprinted from *J. Mater. Sci. Technol.*, 61, X.Z. Wang, H.Q. Fan, T. Muneshwar, K. Cadien, and J.L. Luo, Balancing the corrosion resistance and through-plane electrical conductivity of Cr coating via oxygen plasma treatment, 75–84, Copyright 2021, with permission from Elsevier. (e1–g) Reprinted with permission from X.Z. Wang, H. Luo, T. Muneshwar, H.Q. Fan, K. Cadien, and J.L. Luo, *ACS Appl. Mater. Interfaces*, 10, 40111–40127 (2018) [62]. Copyright 2018 American Chemical Society. (h–j) Reprinted from *J. Power Sources*, 397, X.Z. Wang, T.P. Muneshwar, H.Q. Fan, K. Cadien, and J.L. Luo, Achieving ultrahigh corrosion resistance and conductive zirconium oxynitride coating on metal bipolar plates by plasma enhanced atomic layer deposition, 32–36, Copyright 2018, with permission from Elsevier.

triangular wave with a potential change range of 1.1–1.6 V vs. SCE within 2 s to accelerate the degradation of the bipolar plate. With the increase of O_2 flow rate, the pace of current density elevation at 1.6 V vs. SCE had slowed down, indicating that the addition of O_2 improved the corrosion resistance and stability of the TiN coating. However, the oxygen-doped TiN coating enhanced the anti-oxidation and anti-corrosion properties while simultaneously weakening the conductivity. Additionally, Hong *et al*. [63] conducted heat treatment on the TiN deposited samples at different temperatures to incorporate O_2 into the coatings. Although the resulting oxide layer effectively reduced corrosion rate, it significantly increased the ICR due to the thicker oxide layer formed at high temperature of 450°C. In contrast, coatings treated at 300°C formed a gradient layer with an appropriate amount of oxide and exhibited a low ICR value of 8.3 and 12.2 mΩ·cm^2 before and after potentiostatic polarization at 0.6 V vs. Ag/AgCl, respectively.

In summary, oxide coatings have the potential to reduce corrosion rates and enhance the chemical stability of the coating. Despite their inherent lower conductivity, the remarkable corrosion resistance of these coatings plays a crucial role in mitigating the rapid ICR increase typically observed during polarization. Consequently, oxide coatings are emerging as a viable material choice for long-term stability and performance in BPs applications.

2.7. Metal compound composite coatings

Metal compound composite coatings, including metal oxides, carbides, and nitrides, have garnered attention for their potential to achieve a balanced performance in terms of corrosion resistance and electrical conductivity [64–69]. These coatings are designed to address the dual requirements of exceptional corrosion resistance and favorable electrical properties in BPs.

A notable study by Wang *et al*. [64] involved the preparation of Ti/(Ti, Cr)N/CrN multilayer coatings on SS316L by arc ion plating technology (Fig. 9(a) and (b)). The ICR of the coated sample measured 4.9 mΩ·cm^2 under a pressure of 1.5 MPa. The enhanced conductivity could be attributed to the high electrical conductivity of the outermost CrN layer. Simultaneously, the occurrence of metal oxide semiconductors was effectively impeded by the internal Ti layer and the formed nitride layer. Additionally, the reduced internal resistance in the cell featuring the multilayer-coated SS316L bipolar plate elevated the maximum output power density to 811.65 mW·cm^{-2} at 1500 mA·cm^{-2}, comparable to that of the cell equipped with a graphite bipolar plate (Fig. 9(c) and (d)). Further research explored the integration of graphene-like carbon bridged nano-Cu clusters within amorphous carbon matrices, resulting in the creation of a dual-structured $C_{18.60}Cr_{0.06}Cu$ (S65) film was fabricated using magnetron sputtering technique (Fig. 9(e) and (f)) [67]. The ICR of the coating was 7.34 mΩ·cm^2 at 1.4 MPa pressure. Additionally, the potentiostatic polarization revealed that the current density of S65 sample was stable at 0.71 μA·cm^{-2} at 0.6 V vs. Ag/AgCl, underscoring the remarkable anti-corrosion properties of S65 sample. With the target current increasing further, the electrochemical impedance of the samples decreased, signifying that S65 exhibited the highest impedance cycle (Fig. 9(g) and (h)).

Pugal Mani *et al*. [65] employed cathodic arc-physical vapor deposition (CA-PVD) technology to deposit single-layer TiN, TiAlN, and multilayer TiN/TiAlN coatings on SS316L (Fig. 9(i)). The TiN/TiAlN multilayer coating exhibits a dense microstructure and an interfacial barrier between the TiN/TiAlN layers. This configuration impedes the diffusion of corrosive ions such as SO_4^{2-} and F^-, consequently enhancing the material's corrosion resistance. It can be observed that, with the increase of polarization time, the ICR values for all of samples rise, stabilizing around 3.5 h (Fig. 9(j) and (k)). The rise in ICR values for TiAlN and TiN/TiAlN coatings after 4 h of polarization study was predominantly ascribed to the formation of a protective passivating aluminum oxide film on both coatings [70–72]. Subsequently, CrN, CrAlN, and the multilayer CrN/CrAlN coatings were fabricated on SS316L using the cathodic arc evaporation-physical vapor deposition (CAE-PVD) system (Fig. 9(l)). These samples were tested in 85wt% H_3PO_4 solution at 140°C, with the CrN/CrAlN coated samples exhibiting a corrosion current density of 0.91 μA·cm^{-2} at 0.6 V vs. Ag/AgCl under the cathode condition of high temperature proton exchange membrane fuel cells (HT-PEMFCs). Compared with other coatings, the CrN/CrAlN coating exhibited the best protective performance against ionic corrosion. Additionally, the ICR of SS316L/CrN/CrAlN increased marginally from 6 to 7 and 9 mΩ·cm^2 in anode and cathode after potentiostatic polarization respectively, displaying outstanding stability (Fig. 9(m)–(n2)) [66].

In summary, metal compound composite coatings have commendable electrical conductivity, corrosion resistance and stability in long-term service (Fig. 10). However, the complex preparation processes of compounds such as nitrides, carbides, and oxides within these composite coatings present a challenge for large-scale production.

2.8. a-C/metal compound composite coatings

"Conductive carbon + metal" composite coatings, such as C/Ti and C/Cr, have been extensively explored due to their comprehensive performance, which benefit from the conductivity of carbon and the corrosion resistance of metals.

Wu *et al*. [73] prepared Cr/a-C coatings on 304 SS by DC magnetron sputtering. The unique interlocking structure between the Cr layer and the a-C layer effectively prevented corrosive liquids from reaching the substrate, reducing corrosion current density to 0.894 μA·cm^{-2}. Wang *et al*. [74] then prepared C/Ti nano-coatings of varying thicknesses on SS316L ($C_{100}Ti_{60}$/SS and $C_{20}Ti_{140}$/SS), with the $C_{100}Ti_{60}$ coating exhibiting superior corrosion resistance and electrical conductivity. This coating maintained its protective capabilities until a potential of 1.13 V vs. Ag/AgCl, beyond which delamination of the C layer led to a significant increase in

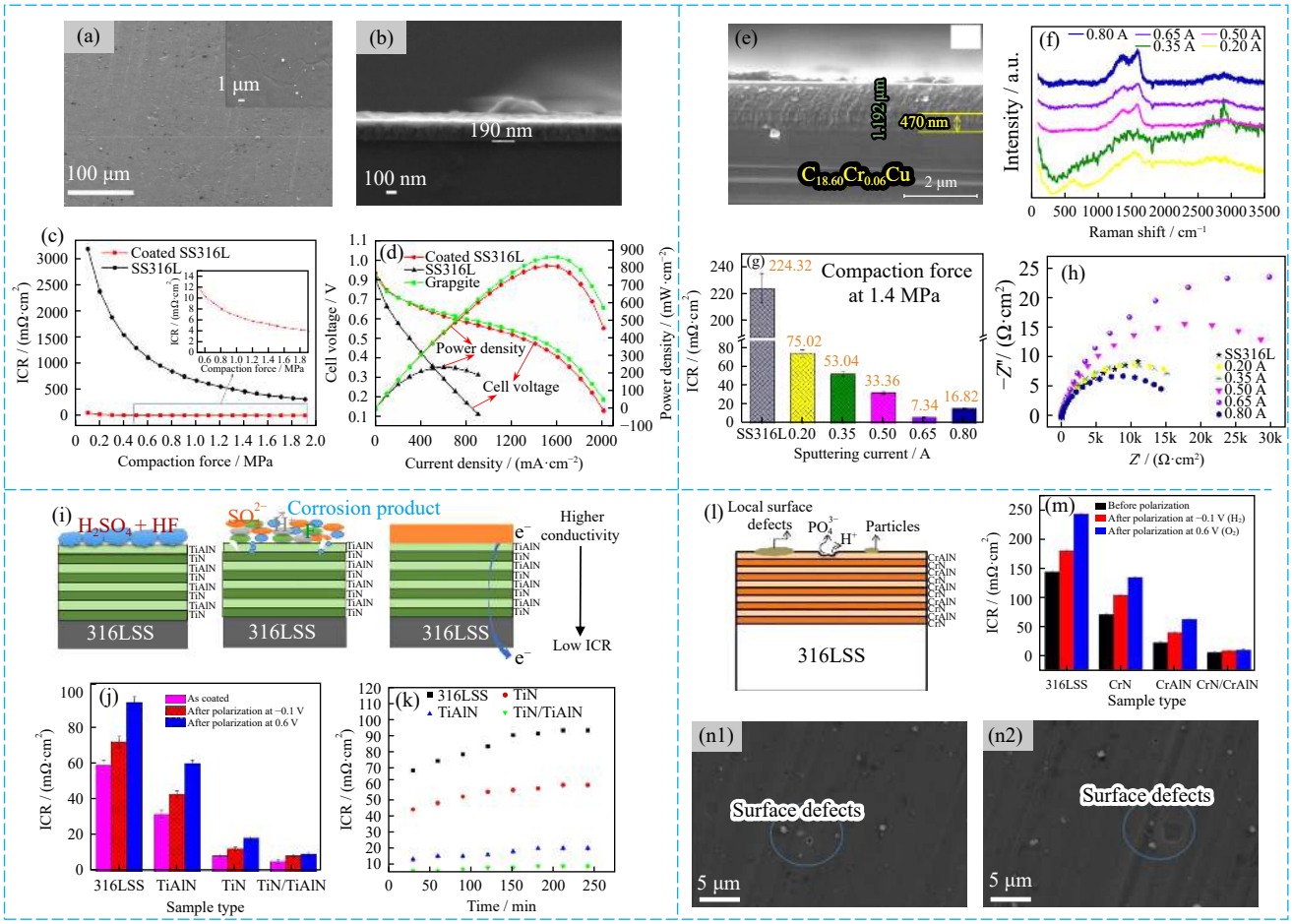

Fig. 9. (a) Surface morphology and (b) SEM image of the multilayer coated SS316L sample; (c) ICR data of coated SS316L and bare SS316L; (d) single cell performances with multilayer coated SS316L, uncoated SS316L and graphite [64]; (e) cross-section of SEM images for S65; (f) Raman spectra of the C_xCr_yCu films; (g) ICR data of different samples at 1.4MPa pressure; (h) Nyquist plots of SS316L and 0.20–0.80 A deposited coatings [67]; (i) corrosion protection mechanism of TiN/TiAlN coatings; (j) ICR values of different samples before and after tests; (k) time vs ICRs after polarization of TiN, TiAlN, and TiN/TiAlN coatings [65]; (l) corrosion protection mechanism of CrN/CrAlN coatings; (m) ICR values of 316SS, CrN, CrAlN, and CrN/CrAlN coatings before and after tests; (n1) and (n2) different position SEM images of CrN/CrAlN/SS after polarization [66]. (a–d) Reprinted from *J. Energy Chem.*, 26, S.L. Wang, M. Hou, Q. Zhao, *et al.*, Ti/(Ti,Cr)N/CrN multilayer coated 316L stainless steel by arc ion plating as bipolar plates for proton exchange membrane fuel cells, 168–174, Copyright 2017, with permission from Elsevier. (e–h) Reprinted from *Mater. Today Chem.*, 21, Q. Jia, Z. Mu, X. Zhang, *et al.*, Electronic conductive and corrosion mechanisms of dual nanostructure CuCr-doped hydrogenated carbon films for SS316L bipolar plates, 100521, Copyright 2021, with permission from Elsevier. (i–k) Reprinted by permission from Springer Nature: *J. Mater. Sci.*, Corrosion resistant and conductive TiN/TiAlN multilayer coating on 316L SS: A promising metallic bipolar plate for proton exchange membrane fuel cell, S. Pugal Mani, M. Kalaiarasan, K. Ravichandran, N. Rajendran, and Y. Meng, Copyright 2021. (l–n2) Reprinted from *J. Mater. Sci. Technol.*, 97, S. Pugal Mani, P. Agilan, M. Kalaiarasan, K. Ravichandran, N. Rajendran, and Y. Meng, Effect of multilayer CrN/CrAlN coating on the corrosion and contact resistance behavior of 316L SS bipolar plate for high temperature proton exchange membrane fuel cell, 134–146, Copyright 2022, with permission from Elsevier.

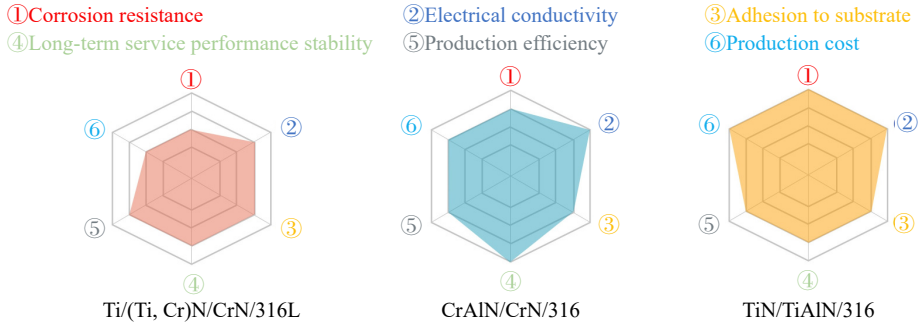

Fig. 10. Performance radar diagrams of three representative metal compound composite coatings.

ICR (266.12 mΩ·cm^2) (Fig. 11(a1)–(a4)). In fact, the substantial rise in ICR is fundamentally attributed to the increase of potential drop within the double electric layer (Fig. 11(b)).

To address the adhesion challenges between carbon and metal interfaces, researchers like Bi *et al*. [75] turned to metal compounds. They synthesized multilayer Zr–C/a-C coatings on SS316L using CFUBMSIP, achieving a stable current density at about 0.06 μA · cm^{-2} after potentiostatic polarization at 0.6 V vs. SCE and a slight increase in ICR from 3.63 to 3.92 mΩ·cm^2. In subsequent work, Bi *et al*. [76] prepared three kinds of a-C coatings with Cr, Ti and Nb as transition layers based on the *E*–pH diagrams to assess the differences in their protective performance on SS316L. The Cr layer promoted graphitization of a-C layer, so the ICR value of Cr transition layer sample was 2.3 mΩ·cm^2, which was less than that of the other two samples. However, Cr suffered from anodic dissolution when the applied potential exceeded 1.2 V vs. SHE, resulting in the outmost a-C layer peeling off. Meanwhile, originating from the Ti and Nb passivation, the a-C coatings with Ti or Nb layers exhibited excellent corrosion resistance even when the applied potential was as high as 1.6 V vs. SHE. It is concluded that a-C coating with Cr layer is recommended for low-potential batteries and a-C coating with Ti or Nb layer could withstand the high-potential shock effectively for batteries under complex working conditions.

Some scholars have prepared composite coatings with multilayer structure. On the one hand, they combined the excellent properties of conductive carbon and metal compounds. On the other hand, multilayer structure could effectively prevent corrosive solutions from interacting with substrates. Yi *et al*. [77] prepared four kinds of multilayer TiC_x/a-C coatings with different thickness of carbon layer on SS316L using CFUBMSIP. With the increase in the thickness (*t*) of the a-C layer, larger graphite like clusters promoted more sp2 hybridized carbon atoms in the layer, while vacancy-like defects became more obvious (Fig. 11(c1)–(e)). The outcomes demonstrate that the 69 nm-sample performed

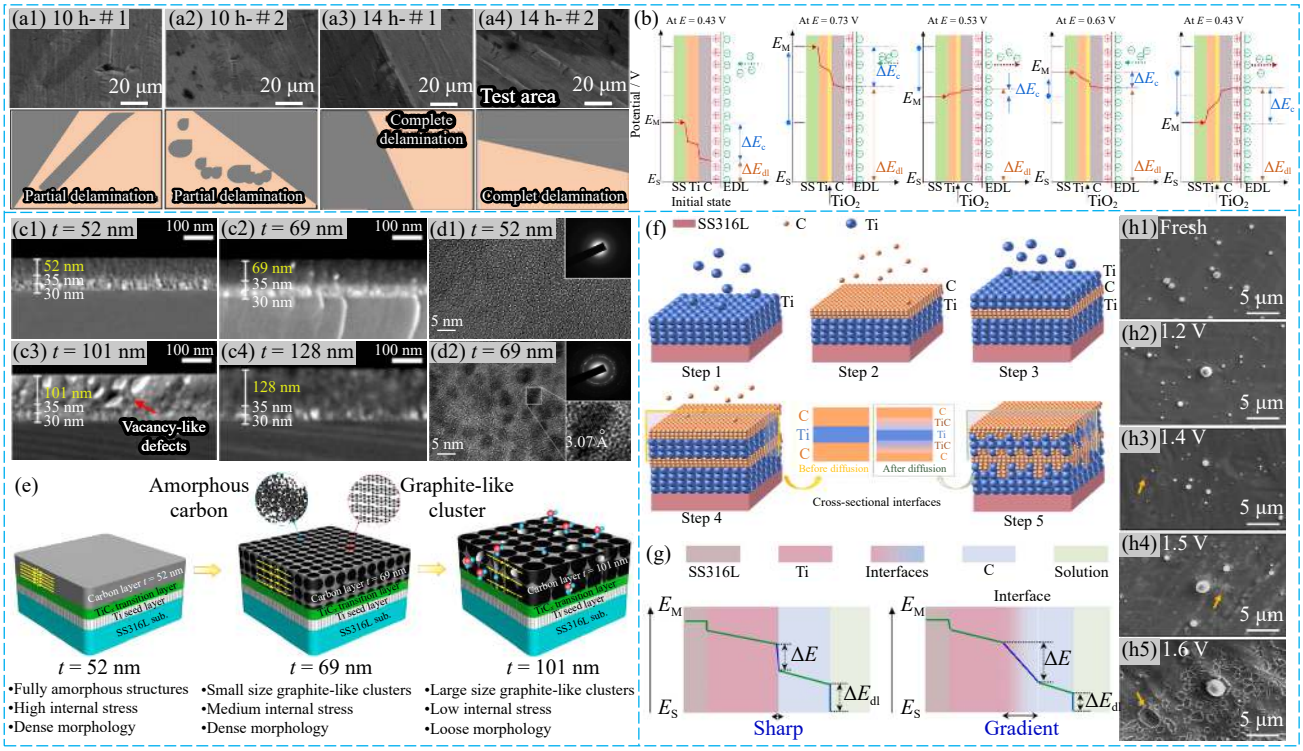

Fig. 11. SEM images and corresponding schematic images of $C_{100}Ti_{60}$/SS after potentiostatic polarization at *E* = 1.33 V for (a1, a2) 10 h and (a3, a4) 14 h; (b) schematically illustration of the potential distribution between the metal substrate, coatings, and the electrical double layer (EDL: electrical double layer, E_M: potential of the metal sample, E_S: potential of the electrolyte solution, ΔE_c: cross-sectional potential drop of the coating layer, ΔE_{dl}: potential difference crosses the double layer) [74]; SEM micrographs of typical samples of (c1) *t* = 52 nm, (c2) *t* = 69 nm, (c3) *t* = 101 nm, and (c4) *t* = 128 nm; (d1–d2) TEM images of the a-C layers and corresponding SAED patterns; (e) schematic diagram of the formation of defects, of internal stress levels, and of the size of graphite-like clusters in a-C layers [77]; (f) schematic illustration of the preparation process of the multilayered C/Ti nanoscale coating; (g) schematic potential distribution across the interfaces of bilayer C/Ti coating (ΔE: the potential drop); (h1–h5) surface morphologies of C/Ti/SS before and after cyclic polarization [79]. (a1–b) Reprinted from *Int. J. Hydrogen Energy*, 47, X.Z. Wang, M.M. Zhang, D.D. Shi, *et al*, Long-term polarization accelerated degradation of nano-thin C/Ti coated SS316L bipolar plates used in polymer electrolyte membrane fuel cells, 8974–8992, Copyright 2022, with permission from Elsevier. (c1–e) Reprinted with permission from P.Y. Yi, D. Zhang, L.F. Peng, and X.M. Lai, *ACS Appl. Mater. Interfaces*, 10, 34561–34572 (2018) [77]. Copyright 2018 American Chemical Society. (f–h5) Reprinted from *Corros. Sci*., 208, X.Z. Wang, M.M. Zhang, Q. Hu, *et al.*, Optimizing the interfacial potential distribution to mitigate high transient potential induced dissolution on C/Ti coated metal bipolar plates used in PEMFCs, 110686, Copyright 2022, with permission from Elsevier.

the best anti-corrosion properties with the stable current density of 0.017 μA·cm^{-2}, attributing to the limited defects and appropriate graphitization. Additionally, the ICR of the coating increased slightly from 2.35 to 5.3 mΩ·cm^2 after the potentiostatic polarization at 0.84 V vs. SHE for 24 h. Zhang *et al*. [78] also prepared a series of multilayer TiC_x/a-C coatings on SS316L by magnetron sputtering, depositing the a-C layers through alternating the negative substrate bias voltage between 150 V and 600 V for *n* periods (*n* = 0, 5, 10, 15). Alternating structure promoted the generation of sp2 rich clusters on the surface and restrained the columnar structures in the a-C layers. As a result, the sample deposited with 15 alternating periods showed optimal performance, with a stable current density about 0.003 μA·cm^{-2} and a low ICR of 6.8 mΩ·cm^2 after potentiostatic polarization at 0.6 V vs. Ag/AgCl.

In addition to these studies, the multilayer C/Ti nano-coatings were fabricated on SS316L and tested their stability with cyclic potentiodynamic and potentiostatic polarization, which simulated the high cathodic transient potential under SU/SD conditions (Fig. 11(f)) [79]. The ICR of the C/Ti/SS reached a significantly low value of 1.59 mΩ·cm^2, and the corrosion current density was 0.02 μA·cm^{-2}, which notably better than the DOE targets. It was found that the diffusion interface between the C and Ti monolayers optimized the potential distribution across the coating and improved the transpassive potential of C/Ti/SS to 1.5 V vs. SHE, thus significantly improving the corrosion resistance of the coating (Fig. 11(g)–(h5)). Yi *et al*. [80] deposited five kinds of multilayer Cr–N–C coatings with different nitrogen content on SS316L by CFUBMSIP using closed-loop optical emission monitor (OEM) to control nitrogen flow rate. The findings suggested that the ICR was mainly determined by the content of C sp2 in a-C layer and the corrosion resistance mainly depended on the content of Cr_3C_2. The S3 sample (sample with OEM values of 60%) achieved optimal properties, with the corrosion current density measuring 0.308 μA·cm^{-2} and the ICR decreasing to 2.11 mΩ·cm^2. Therefore, the content of C sp2 and Cr_3C_2 could be further increased by optimizing the coating process parameters to achieve higher properties. Moreover, Yan *et al*. [81] prepared (a-C: H/TiC)/(TiCN)/(TiN) multilayer coatings on titanium substrate. The columnar crystals disappeared and changed to dense structure with higher C_2H_2 flow rate, which reduced the permeation channels for corrosive ions and helped to improve the corrosion performance. The I_{corr} of the coatings with highest acetylene flow rates of 60 mL·min^{-1} was 0.66 μA·cm^{-2} at 0.6 V vs. SCE. Furthermore, the ICR of a-C multilayer coatings containing a large amount of C sp2 was 1.6 mΩ·cm^2, showing superb conductivity.

In summary, the a-C/metal compound composite coatings exhibit excellent corrosion resistance and outstanding conductivity (Fig. 12), contributing to enhanced efficiency and longevity of PEMFCs. The coating process is relatively straightforward, resulting in reduced raw material costs and suitability for large-scale production, which is also why it stands out as one of the most promising coatings for practical applications.

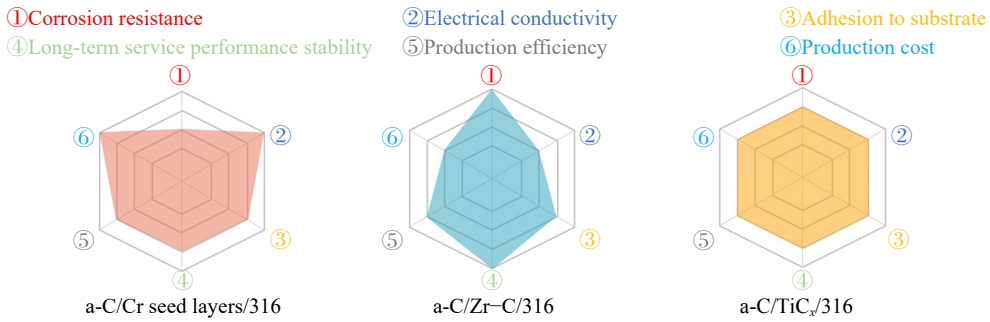

Fig. 12. Performance radar diagrams of three representative a-C/metal compound composite coatings.

2.9. Summary

To intuitively observe the performance differences between various coatings, the comparison of coatings is summarized in Fig. 13 from the perspectives of current density and ICR, particularly the deterioration of conductivity during long-term polarization. Notably, Fig. 13(b) presents a coordinate system in which the proximity of points to the origin correlates with the superior stability of the ICR for the respective layer types. It can be observed that the initial ICR of oxide coatings is relatively high, potentially due to the limited availability of free electrons within their matrix and the inherent characteristics of their crystalline structure and chemical bonding. Additionally, metal compound coatings have demonstrated superior comprehensive performance, making them a relatively viable option for metallic BPs coatings. At last, it is worth noting that both in Fig. 13(a) and (b), most of the a-C/metal coating data are close to the origin, demonstrating robust comprehensive performance, which is why a-C/metal coatings are considered to be the most promising option for metallic BPs.

3. Conclusions and outlook

This review offers a comprehensive analysis of the latest advancements in coatings for PEMFCs metal bipolar plates, underscoring the universal objective of achieving a balance between high electrical conductivity and excellent corrosion resistance. This endeavor is crucial for meeting the technical benchmarks established by the Department of Energy (DOE). The results permit the following conclusions:

(1) Polymer coatings: The conductivity and corrosion res-

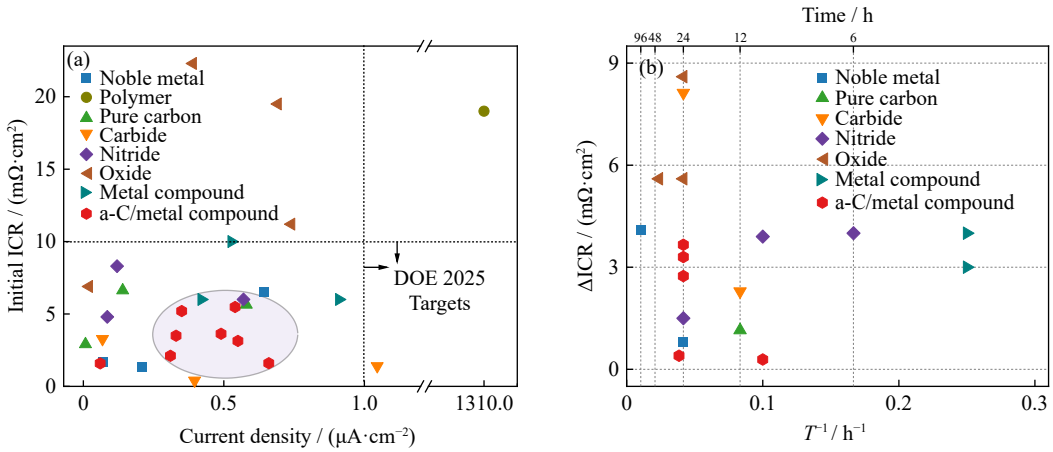

Fig. 13. (a) Diagram of ICR at 1.4 MPa pressure and current density at 0.84 V vs. SHE of different coatings and (b) variation of ΔICR with time and 1/*T* of different coatings.

istance are far from the basic requirements. There is a need to optimize overall performance and increase polymerization efficiency for practical application.

(2) Noble metal coatings: These coatings have remarkable and stable conductivity. However, the high production cost limits their suitability for mass production. Future research should focus on minimizing the use of noble metals while avoiding galvanic corrosion to maintain their comprehensive performance.

(3) Pure carbon coatings: The carbon coating is relatively stable in acid environment and has available initial conductivity. But the coating is easy to fall off and crack due to the lack of adhesion with metal substrate. The high cost caused by the low deposition rate of carbon also needs to be solved.

(4) Carbide coatings: For most carbide coatings, the limited corrosion resistance causes a significant deterioration in conductivity after polarization. Future challenges include finding suitable metal carbides with prominent properties and maintaining electrical conductivity over extended service times.

(5) Nitride coatings: This kind of coating possesses good corrosion resistance and initial electrical conductivity, which can meet the basic requirements. However, issues with conductivity loss due to corrosion dissolution in acidic solutions and oxidation of coatings need addressing.

(6) Oxide coatings: Benefiting from the high transpassivation potential of oxides, these coatings generally show good corrosion resistance at high potential. Nevertheless, exploring suitable oxygen content to achieve improved initial conductivity and ensure long-term performance remains a significant challenge.

(7) Metal compound composite coatings: In order to combine the available characteristics of various metal compounds, the design of coatings is generally cumbersome. The low efficiency in preparing these compounds is a barrier to large-scale production, necessitating process optimization.

(8) a-C/metal compound composite coatings: Combined with the remarkable conductivity of a-C layer and the corrosion resistance of metal, this kind of coating has balanced performance and basically meets the requirements of practical application. In particular, the conductivity decay in the long-term polarization has been mitigated. Improvements are needed in carbon layer stability at high potentials and coating corrosion resistance under transient service conditions.

In general, despite substantial strides in this field, several overarching challenges persist, encompassing the enhancement of coating durability, efficiency in preparation, cost reduction, and scalability for mass production. A pivotal concern across all coatings is the significant increase in ICR under simulated corrosion conditions, impacting their practical viability. Additionally, adopting more realistic testing methods in actual PEMFCs conditions, such as long-term dynamic polarization and high transient potential polarization, is crucial for accurately evaluating the lifetime and durability of various coatings.

Acknowledgements

The authors wish to acknowledge the support from the Shenzhen Science and Technology Program of China (No. JCYJ20220530161614031), National Natural Science Foundation of China (No. 52471094), and Shaanxi Coal Chemical Industry Technology Research Institute Co., Ltd.

Conflict of Interest

All authors do not have competing interests to declare.

Supplementary Information

The online version contains supplementary material available at https://doi.org/10.1007/ s12613-024-2946-0.

References

[1] K. Jiao, J. Xuan, Q. Du, *et al*., Designing the next generation of proton-exchange membrane fuel cells, *Nature*, 595(2021), No. 7867, p. 361.

[2] G.Y. Liu, F.G. Hou, S.L. Peng, X.D. Wang, and B.Z. Fang, Process and challenges of stainless steel based bipolar plates for proton exchange membrane fuel cells, *Int. J. Miner. Metall. Mater.*, 29(2022), No. 5, p. 1099.

[3] Y. Wang, D.F. Ruiz Diaz, K.S. Chen, Z. Wang, and X.C. Adro-

her, Materials, technological status, and fundamentals of PEM fuel cells–A review, *Mater. Today*, 32(2020), p. 178.
[4] Z.T. Xu, D.K. Qiu, P.Y. Yi, L.F. Peng, and X.M. Lai, Towards mass applications: A review on the challenges and developments in metallic bipolar plates for PEMFC, *Prog. Nat. Sci. Mater. Int.*, 30(2020), No. 6, p. 815.
[5] R. Włodarczyk, Corrosion analysis of graphite sinter as bipolar plates in the low-temperature PEM fuel cell simulated environments, *J. Solid State Electrochem.*, 26(2022), No. 1, p. 39.
[6] S. Simaafrookhteh, M. Khorshidian, and M. Momenifar, Fabrication of multi-filler thermoset-based composite bipolar plates for PEMFCs applications: Molding defects and properties characterizations, *Int. J. Hydrogen Energy*, 45(2020), No. 27, p. 14119.
[7] X.B. Li, L.F. Peng, D. Zhang, P.Y. Yi, and X.M. Lai, The frequency of pulsed DC sputtering power introducing the graphitization and the durability improvement of amorphous carbon films for metallic bipolar plates in proton exchange membrane fuel cells, *J. Power Sources*, 466(2020), art. No. 228346.
[8] A.P. Pitchiya, N.T. Le, Z.A. Putnam, M. Harrington, and S. Krishnan, Microporous graphite composites of tailorable porosity, surface wettability, and water permeability for fuel cell bipolar plates, *Ind. Eng. Chem. Res.*, 60(2021), No. 28, p. 10203.
[9] H.E. Lee, Y.S. Chung, and S.S. Kim, Feasibility study on carbon-felt-reinforced thermoplastic composite materials for PEMFC bipolar plates, *Compos. Struct.*, 180(2017), p. 378.
[10] X.Z. Wang, C.P. Ye, D.D. Shi, H.Q. Fan, and Q. Li, Potential polarization accelerated degradation of interfacial electrical conductivity for Au/TiN coated 316L SS bipolar plates used in polymer electrolyte membrane fuel cells, *Corros. Sci.*, 189(2021), art. No. 109624.
[11] L.X. Yang, R.J. Liu, Y. Wang, H.J. Liu, C.L. Zeng, and C. Fu, Growth of nanocrystalline β-Nb_2N coating on 430 ferritic stainless steel bipolar plates of PEMFCs by disproportionation reaction of Nb(IV) ions in molten salt, *Corros. Sci.*, 174(2020), art. No. 108862.
[12] Z.T. Xu, Z.P. Li, R. Zhang, T.H. Jiang, and L.F. Peng, Fabrication of micro channels for titanium PEMFC bipolar plates by multistage forming process, *Int. J. Hydrogen Energy*, 46(2021), No. 19, p. 11092.
[13] N.F. Asri, T. Husaini, A.B. Sulong, E.H. Majlan, and W.R.W. Daud, Coating of stainless steel and titanium bipolar plates for anticorrosion in PEMFC: A review, *Int. J. Hydrogen Energy*, 42(2017), No. 14, p. 9135.
[14] Y.W. Zeng, Z.H. He, Q.H. Hua, Q.J. Xu, and Y.L. Min, Polyacrylonitrile infused in a modified honeycomb aluminum alloy bipolar plate and its acid corrosion resistance, *ACS Omega*, 5(2020), No. 27, p. 16976.
[15] Y. Sim, J. Kwak, S.Y. Kim, *et al*., Formation of 3D graphene–Ni foam heterostructures with enhanced performance and durability for bipolar plates in a polymer electrolyte membrane fuel cell, *J. Mater. Chem. A*, 6(2018), No. 4, p. 1504.
[16] T. Wilberforce, O. Ijaodola, E. Ogungbemi, *et al*., Technical evaluation of proton exchange membrane (PEM) fuel cell performance–A review of the effects of bipolar plates coating, *Renewable Sustainable Energy Rev.*, 113(2019), art. No. 109286.
[17] F. Madadi, A. Rezaeian, H. Edris, and M. Zhiani, Improving performance in PEMFC by applying different coatings to metallic bipolar plates, *Mater. Chem. Phys.*, 238(2019), art. No. 121911.
[18] L. Jiang, J.A. Syed, H.B. Lu, and X.K. Meng, *In-situ* electrodeposition of conductive polypyrrole–graphene oxide composite coating for corrosion protection of 304SS bipolar plates, *J. Alloys Compd.*, 770(2019), p. 35.
[19] S. Liu, T.J. Pan, R.F. Wang, Y. Yue, and J. Shen, Anti-corrosion and conductivity of the electrodeposited graphene/polypyrrole composite coating for metallic bipolar plates, *Prog. Org. Coat.*, 136(2019), art. No. 105237.
[20] Z.H. Chen, G.H. Zhang, W.Z. Yang, *et al*., Superior conducting polypyrrole anti-corrosion coating containing functionalized carbon powders for 304 stainless steel bipolar plates in proton exchange membrane fuel cells, *Chem. Eng. J.*, 393(2020), art. No. 124675.
[21] S. Akula, P. Kalaiselvi, A.K. Sahu, and S. Chellammal, Electrodeposition of conductive PAMT/PPY bilayer composite coatings on 316L stainless steel plate for PEMFC application, *Int. J. Hydrogen Energy*, 46(2021), No. 34, p. 17909.
[22] S. Joseph, J.C. McClure, P.J. Sebastian, J. Moreira, and E. Valenzuela, Polyaniline and polypyrrole coatings on aluminum for PEM fuel cell bipolar plates, *J. Power Sources*, 177(2008), No. 1, p. 161.
[23] L.J. Yang, H.J. Yu, L.J. Jiang, L. Zhu, X.Y. Jian, and Z. Wang, Graphite–polypyrrole coated 316L stainless steel as bipolar plates for proton exchange membrane fuel cells, *Int. J. Miner. Metall. Mater.*, 18(2011), No. 1, p. 53.
[24] Y.L. Wang, S.H. Zhang, P. Wang, Z.X. Lu, S.B. Chen, and L.S. Wang, Synthesis and corrosion protection of Nb doped TiO_2 nanopowders modified polyaniline coating on 316 stainless steel bipolar plates for proton-exchange membrane fuel cells, *Prog. Org. Coat.*, 137(2019), art. No. 105327.
[25] Y.L. Wang, S.H. Zhang, P. Wang, S.B. Chen, Z.X. Lu, and W.H. Li, Electropolymerization and corrosion protection performance of the Nb: TiO_2 nanofibers/polyaniline composite coating, *J. Taiwan Inst. Chem. Eng.*, 103(2019), p. 190.
[26] M. Ates and E. Topkaya, Nanocomposite film formations of polyaniline via TiO_2, Ag, and Zn, and their corrosion protection properties, *Prog. Org. Coat.*, 82(2015), p. 33.
[27] M.A. Deyab, Corrosion protection of aluminum bipolar plates with polyaniline coating containing carbon nanotubes in acidic medium inside the polymer electrolyte membrane fuel cell, *J. Power Sources*, 268(2014), p. 50.
[28] N.D. Nam, J.G. Kim, Y.J. Lee, and Y.K. Son, Effect of thermal treatment on the corrosion resistance of polyaniline in H_2SO_4–HF acid mixture solution, *Corros. Sci.*, 51(2009), No. 12, p. 3007.
[29] K.J. Lin, X.Y. Li, H.S. Dong, *et al*., Surface modification of 316 stainless steel with platinum for the application of bipolar plates in high performance proton exchange membrane fuel cells, *Int. J. Hydrogen Energy*, 42(2017), No. 4, p. 2338.
[30] W.M. Yan, C.Y. Chen, and C.H. Liang, Comparison of performance degradation of high temperature PEM fuel cells with different bipolar plates, *Energy*, 186(2019), art. No. 115836.
[31] F.Y. Yan, B.L. Jiang, Z.Y. Wang, *et al*., Thermal stabilization of nanocrystalline promoting conductive corrosion resistance of TiN–Ag films for metal bipolar plates, *Vacuum*, 195(2022), art. No. 110631.
[32] D. Zhang, P.Y. Yi, L.F. Peng, X.M. Lai, and J.B. Pu, Amorphous carbon films doped with silver and chromium to achieve ultra-low interfacial electrical resistance and long-term durability in the application of proton exchange membrane fuel cells, *Carbon*, 145(2019), p. 333.
[33] M. Liu, H.F. Xu, J. Fu, and Y. Tian, Conductive and corrosion behaviors of silver-doped carbon-coated stainless steel as PEMFC bipolar plates, *Int. J. Miner. Metall. Mater.*, 23(2016), No. 7, p. 844.
[34] T. Fukutsuka, T. Yamaguchi, S.I. Miyano, Y. Matsuo, Y. Sugie, and Z. Ogumi, Carbon-coated stainless steel as PEFC bipolar plate material, *J. Power Sources*, 174(2007), No. 1, p. 199.
[35] A. Afshar, M. Yari, M.M. Larijani, and M. Eshghabadi, Effect of substrate temperature on structural properties and corrosion resistance of carbon thin films used as bipolar plates in polymer electrolyte membrane fuel cells, *J. Alloys Compd.*, 502(2010), No. 2, p. 451.
[36] H. Li, P. Guo, D. Zhang, *et al*., Interface-induced degradation of

amorphous carbon films/stainless steel bipolar plates in proton exchange membrane fuel cells, *J. Power Sources*, 469(2020), art. No. 228269.
[37] W.L. Wang, S.M. He, and C.H. Lan, Protective graphite coating on metallic bipolar plates for PEMFC applications, *Electrochim. Acta*, 62(2012), p. 30.
[38] L.X. Li, D.H. Ye, Y. Xiang, and W. Guo, Effect of deposition temperature on columnar structure of α-C nano-coatings of PEMFC metal bipolar plates, *Int. J. Electrochem. Sci.*, 18(2023), No. 7, art. No. 100188.
[39] I. Alaefour, S. Shahgaldi, J. Zhao, and X.G. Li, Synthesis and *Ex-situ* characterizations of diamond-like carbon coatings for metallic bipolar plates in PEM fuel cells, *Int. J. Hydrogen Energy*, 46(2021), No. 19, p. 11059.
[40] P.Y. Yi, W.X. Zhang, F.F. Bi, L.F. Peng, and X.M. Lai, Microstructure and properties of a-C films deposited under different argon flow rate on stainless steel bipolar plates for proton exchange membrane fuel cells, *J. Power Sources*, 410(2019), p. 188.
[41] W. Li, L.T. Liu, Z.X. Li, Y.F. Wang, H.Z. Li, and J.J. Lei, Corrosion resistance and conductivity of amorphous carbon coated SS316L and TA2 bipolar plates in proton-exchange membrane fuel cells, *Diamond Relat. Mater.*, 118(2021), art. No. 108503.
[42] J. Jin, X.L. Kou, X. Tian, *et al*., Investigation of corrosion protection with conductive chromium–aluminum carbonitride coating on metallic bipolar plates, *Vacuum*, 213(2023), art. No. 112084.
[43] L. Wang, Y.K. Tao, Z. Zhang, *et al*., Molybdenum carbide coated 316L stainless steel for bipolar plates of proton exchange membrane fuel cells, *Int. J. Hydrogen Energy*, 44(2019), No. 10, p. 4940.
[44] Y. Zhao, L. Wei, P.Y. Yi, and L.F. Peng, Influence of Cr–C film composition on electrical and corrosion properties of 316L stainless steel as bipolar plates for PEMFCs, *Int. J. Hydrogen Energy*, 41(2016), No. 2, p. 1142.
[45] K. Hou, P.Y. Yi, X.B. Li, L.F. Peng, and X.M. Lai, The effect of Cr doped in amorphous carbon films on electrical conductivity: Characterization and mechanism, *Int. J. Hydrogen Energy*, 46(2021), No. 60, p. 30841.
[46] J.L. Lu, N. Abbas, J.N. Tang, J. Tang, and G.M. Zhu, Synthesis and characterization of conductive ceramic MAX-phase coatings for metal bipolar plates in simulated PEMFC environments, *Corros. Sci.*, 158(2019), art. No. 108106.
[47] G.S. Ma, D. Zhang, P. Guo, *et al*., Phase orientation improved the corrosion resistance and conductivity of Cr_2AlC coatings for metal bipolar plates, *J. Mater. Sci. Technol.*, 105(2022), p. 36.
[48] H.B. Zhang, K. Jiang, Y. Qiu, *et al*., Electrochemical properties of niobium and niobium compounds modified AISI430 stainless steel as bipolar plates for DFAFC, *Surf. Eng.*, 35(2019), No. 11, p. 1003.
[49] T. Taner, S.A.H. Naqvi, and M. Ozkaymak, Techno-economic analysis of a more efficient hydrogen generation system prototype: A case study of PEM electrolyzer with Cr–C coated SS304 bipolar plates, *Fuel Cells*, 19(2019), No. 1, p. 19.
[50] J. Bi, J.M. Yang, X.X. Liu, *et al*., Development and evaluation of nitride coated titanium bipolar plates for PEM fuel cells, *Int. J. Hydrogen Energy*, 46(2021), No. 1, p. 1144.
[51] T.J. Pan, Y.J. Dai, J. Jiang, J.H. Xiang, Q.Q. Yang, and Y.S. Li, Anti-corrosion performance of the conductive bilayer CrC/CrN coated 304SS bipolar plate in acidic environment, *Corros. Sci.*, 206(2022), art. No. 110495.
[52] L.X. Yang, R.J. Liu, Y. Wang, H.J. Liu, C.L. Zeng, and C. Fu, Corrosion and interfacial contact resistance of nanocrystalline β-Nb_2N coating on 430 FSS bipolar plates in the simulated PEMFC anode environment, *Int. J. Hydrogen Energy*, 46(2021), No. 63, p. 32206.
[53] Y. Jang, Y. Kim, W. Jeong, *et al*., Corrosion behavior of Ta and TiN double-layer-coated SUS316L for PEMFC bipolar plates using plasma-enhanced atomic layer deposition and magnetron sputtering, *J. Alloys Compd.*, 977(2024), art. No. 173379.
[54] W.J. Lee, E.Y. Yun, H.B.R. Lee, S.W. Hong, and S.H. Kwon, Ultrathin effective TiN protective films prepared by plasma-enhanced atomic layer deposition for high performance metallic bipolar plates of polymer electrolyte membrane fuel cells, *Appl. Surf. Sci.*, 519(2020), art. No. 146215.
[55] B.S. Mi, Z. Chen, Q. Wang, Y. Li, Z.W. Qin, and H.B. Wang, Properties of C-doped CrTiN films on the 316L stainless steel bipolar plate for PEMFC, *Int. J. Hydrogen Energy*, 46(2021), No. 64, p. 32645.
[56] L.H. Yang, Z.L. Qin, H.T. Pan, H. Yun, Y.L. Min, and Q.J. Xu, Corrosion protection of 304 stainless steel bipolar plates of PEMFC by coating SnO_2 film, *Int. J. Electrochem. Sci.*, 12(2017), No. 11, p. 10946.
[57] Y.L. Wang, S.H. Zhang, Z.X. Lu, L.S. Wang, and W.H. Li, Preparation and performances of electrically conductive Nb-doped TiO_2 coatings for 316 stainless steel bipolar plates of proton-exchange membrane fuel cells, *Corros. Sci.*, 142(2018), p. 249.
[58] M.F. Pillis, M.C.L. Oliveira, and R.A. Antunes, Surface chemistry and the corrosion behavior of magnetron sputtered niobium oxide films in sulfuric acid solution, *Appl. Surf. Sci.*, 462(2018), p. 344.
[59] X.Z. Wang, H.Q. Fan, T. Muneshwar, K. Cadien, and J.L. Luo, Balancing the corrosion resistance and through-plane electrical conductivity of Cr coating via oxygen plasma treatment, *J. Mater. Sci. Technol.*, 61(2021), p. 75.
[60] J. Jin, M.L. Hu, and X.H. Zhao, Investigation of incorporating oxygen into TiN coating to resist high potential effects on PEMFC bipolar plates in vehicle applications, *Int. J. Hydrogen Energy*, 45(2020), No. 43, p. 23310.
[61] X.Z. Wang, T.P. Muneshwar, H.Q. Fan, K. Cadien, and J.L. Luo, Achieving ultrahigh corrosion resistance and conductive zirconium oxynitride coating on metal bipolar plates by plasma enhanced atomic layer deposition, *J. Power Sources*, 397(2018), p. 32.
[62] X.Z. Wang, H. Luo, T. Muneshwar, H.Q. Fan, K. Cadien, and J.L. Luo, Zr_2N_2O coating-improved corrosion resistance for the anodic dissolution induced by cathodic transient potential, *ACS Appl. Mater. Interfaces*, 10(2018), No. 46, p. 40111.
[63] Y.Y. Hong, X.Z. Wang, K. Cadien, and J.L. Luo, Controlled oxygen incorporation in TiN coatings via heat treatment for applications in PEMFC metallic bipolar plates, *J. Electrochem. Soc.*, 168(2021), No. 5, art. No. 051502.
[64] S.L. Wang, M. Hou, Q. Zhao, *et al*., Ti/(Ti, Cr)N/CrN multilayer coated 316L stainless steel by arc ion plating as bipolar plates for proton exchange membrane fuel cells, *J. Energy Chem.*, 26(2017), No. 1, p. 168.
[65] S. Pugal Mani, M. Kalaiarasan, K. Ravichandran, N. Rajendran, and Y. Meng, Corrosion resistant and conductive TiN/TiAlN multilayer coating on 316L SS: A promising metallic bipolar plate for proton exchange membrane fuel cell, *J. Mater. Sci.*, 56(2021), No. 17, p. 10575.
[66] S. Pugal Mani, P. Agilan, M. Kalaiarasan, K. Ravichandran, N. Rajendran, and Y. Meng, Effect of multilayer CrN/CrAlN coating on the corrosion and contact resistance behavior of 316L SS bipolar plate for high temperature proton exchange membrane fuel cell, *J. Mater. Sci. Technol.*, 97(2022), p. 134.
[67] Q. Jia, Z. Mu, X. Zhang, *et al*., Electronic conductive and corrosion mechanisms of dual nanostructure CuCr-doped hydrogenated carbon films for SS316L bipolar plates, *Mater. Today Chem.*, 21(2021), art. No. 100521.
[68] J. Jin, J.Z. Zhang, M.L. Hu, and X. Li, Investigation of high potential corrosion protection with titanium carbonitride coating on 316L stainless steel bipolar plates, *Corros. Sci.*, 191(2021), art. No. 109757.

[69] S. Peng, J. Xu, Z.Y. Li, *et al*., A reactive-sputter-deposited TiSiN nanocomposite coating for the protection of metallic bipolar plates in proton exchange membrane fuel cells, *Ceram. Int.*, 46(2020), No. 3, p. 2743.

[70] A.H. Liu, J.X. Deng, H.B. Cui, Y.Y. Chen, and J. Zhao, Friction and wear properties of TiN, TiAlN, AlTiN and CrAlN PVD nitride coatings, *Int. J. Refract. Met. Hard Mater.*, 31(2012), p. 82.

[71] M. Dadfar, M. Salehi, M.A. Golozar, and S. Trasatti, Surface modification of 304 stainless steels to improve corrosion behavior and interfacial contact resistance of bipolar plates, *Int. J. Hydrogen Energy*, 41(2016), No. 46, p. 21375.

[72] Y.H. Lee, S. Noh, J.H. Lee, S.H. Chun, S.W. Cha, and I. Chang, Durable graphene-coated bipolar plates for polymer electrolyte fuel cells, *Int. J. Hydrogen Energy*, 42(2017), No. 44, p. 27350.

[73] M.G. Wu, C.D. Lu, T. Hong, *et al*., Chromium interlayer amorphous carbon film for 304 stainless steel bipolar plate of proton exchange membrane fuel cell, *Surf. Coat. Technol.*, 307(2016), p. 374.

[74] X.Z. Wang, M.M. Zhang, D.D. Shi, *et al*, Long-term polarization accelerated degradation of nano-thin C/Ti coated SS316L bipolar plates used in polymer electrolyte membrane fuel cells, *Int. J. Hydrogen Energy*, 47(2022), No. 14, p. 8974.

[75] F.F. Bi, L.F. Peng, P.Y. Yi, and X.M. Lai, Multilayered Zr–C/a-C film on stainless steel 316L as bipolar plates for proton exchange membrane fuel cells, *J. Power Sources*, 314(2016), p. 58.

[76] F.F. Bi, X.B. Li, P.Y. Yi, K. Hou, L.F. Peng, and X.M. Lai, Characteristics of amorphous carbon films to resist high potential impact in PEMFCs bipolar plates for automotive application, *Int. J. Hydrogen Energy*, 42(2017), No. 20, p. 14279.

[77] P.Y. Yi, D. Zhang, L.F. Peng, and X.M. Lai, Impact of film thickness on defects and the graphitization of nanothin carbon coatings used for metallic bipolar plates in proton exchange membrane fuel cells, *ACS Appl. Mater. Interfaces*, 10(2018), No. 40, p. 34561.

[78] W.X. Zhang, P.Y. Yi, L.F. Peng, and X.M. Lai, Strategy of alternating bias voltage on corrosion resistance and interfacial conductivity enhancement of TiC_x/a-C coatings on metallic bipolar plates in PEMFCs, *Energy*, 162(2018), p. 933.

[79] X.Z. Wang, M.M. Zhang, Q. Hu, *et al*., Optimizing the interfacial potential distribution to mitigate high transient potential induced dissolution on C/Ti coated metal bipolar plates used in PEMFCs, *Corros. Sci.*, 208(2022), art. No. 110686.

[80] P.Y. Yi, L.F. Peng, T. Zhou, J.Q. Huang, and X.M. Lai, Composition optimization of multilayered chromium-nitride–carbon film on 316L stainless steel as bipolar plates for proton exchange membrane fuel cells, *J. Power Sources*, 236(2013), p. 47.

[81] W.Q. Yan, Y.F. Zhang, L. Chen, *et al*., Corrosion behavior and interfacial conductivity of amorphous hydrogenated carbon and titanium carbide composite (a-C:H/TiC) films prepared on titanium bipolar plates in PEMFCs, *Diamond Relat. Mater.*, 120(2021), art. No. 108628.